Testing of a Stitched Composite Large-Scale Multi-Bay Pressure Box

Dawn Jegley,[1] Marshall Rouse,[2] Adam Przekop,[1] Andrew Lovejoy[1]
NASA Langley Research Center, Hampton, VA 23681

NASA has created the Environmentally Responsible Aviation (ERA) Project to develop technologies to reduce aviation's impact on the environment. A critical aspect of this pursuit is the development of a lighter, more robust airframe to enable the introduction of unconventional aircraft configurations. NASA and The Boeing Company have worked together to develop a structural concept that is lightweight and an advancement beyond state-of-the-art composite structures. The Pultruded Rod Stitched Efficient Unitized Structure (PRSEUS) is an integrally stiffened panel design where elements are stitched together. The PRSEUS concept is designed to maintain residual load carrying capabilities under a variety of damage scenarios. A series of building block tests were evaluated to explore the fundamental assumptions related to the capability and advantages of PRSEUS panels. The final step in the building block series is an 80%-scale pressure box representing a portion of the center section of a Hybrid Wing Body (HWB) transport aircraft. The testing of this article under maneuver load and internal pressure load conditions is the subject of this paper. The experimental evaluation of this article, along with the other building block tests and the accompanying analyses, has demonstrated the viability of a PRSEUS center body for the HWB vehicle. Additionally, much of the development effort is also applicable to traditional tube-and-wing aircraft, advanced aircraft configurations, and other structures where weight and through-the-thickness strength are design considerations.

I. Introduction

NASA has created the Environmentally Responsible Aviation (ERA) Project to explore and document the feasibility, benefits, and technical risk of advanced vehicle configurations and enabling technologies to reduce impact of aviation operations on the environment. A critical aspect of this pursuit is the development of a lighter, more robust airframe to enable the introduction of unconventional aircraft configurations that have higher lift to drag ratios, reduce drag, and lower community noise. The Hybrid Wing Body (HWB) configuration is a significant improvement in aerodynamic performance compared to the traditional tube-and-wing aircraft. However, the HWB configuration poses challenges in the design of a non-circular pressure cabin that is lightweight and economical to produce. Developing a structural concept that supports the HWB cabin design is the primary technical challenge to the implementation of a large lifting body design like the HWB.[1]

To address this challenge, researchers at NASA and The Boeing Company (Boeing) have worked together to develop a new structural concept called the Pultruded Rod Stitched Efficient Unitized Structure (PRSEUS).[2-5] In ERA and previous programs, the PRSEUS concept was evaluated analytically and experimentally using a building-block approach.[6-12] As the final step in a building-block process, a 30-foot-long multi-bay pressure box (MBB) has been constructed which contains 11 PRSEUS panels. This pressure box test article has been subjected to a series of loadings. The testing of this large-scale test article is the subject of this paper. Details describing this testing effort can be found in Ref. 13 and 14.

[1] Senior Aerospace Research Engineer, Structural Mechanics and Concepts Branch, Mail Stop 190, 8 West Taylor Street, Associate Fellow AIAA.
[2] Senior Aerospace Research Engineer, Structural Testing Branch, Mail Stop 190, 8 West Taylor Street. Senior Member AIAA.

II. HWB Structural Design

While the HWB provides many aerodynamic advantages, it presents challenges to the structural design of the center fuselage section due to the non-circular shape of the HWB, as shown in the aircraft image in Fig. 1. Although significantly lighter than conventional aluminum structures, even the most highly efficient composite primary structures used on today's state of the art aircraft would not be adequate to overcome the weight and cost penalties introduced by the highly contoured airframe of the HWB. A particularly difficult region to address is the pressure cabin where design is driven by out-of-plane loading considerations. In this region, a traditional layered material system would require thousands of mechanical attachments to suppress delaminations and to join structural elements, ultimately leading to fastener pull through as a critical failure mode in the thin-gauge skins. Another disadvantage of a conventional composite structure for this application is the high manufacturing costs associated with the highly contoured airframe. The essential characteristics of a more capable HWB structural solution are ones that operate effectively in out-of-plane loading scenarios, while simultaneously meeting the demanding producibility requirements inherent in building a highly contoured airframe.

In addition to the bending stresses experienced during pressurization, another key difference between the HWB shell and the traditional cylindrical fuselage is the unique bi-axial loading pattern that occurs during maneuver loading conditions, as shown in Fig. 1. For the HWB, the load magnitudes are nearly equal in each in-plane direction (Nx and Ny), which is in contrast to the loading that is typically found in conventional tube and wing fuselage arrangements, where the cantilevered fuselage is more highly loaded in the Nx direction, along the stringer, than in the Ny direction, along the frame. This single difference has a profound effect on the structural concept selection because this loading arrangement dictates that the optimum panel geometry should have continuous load paths in both directions (Nx and Ny), in addition to efficiently transmitting internal pressure loads (Nz) for the near-flat panel geometry, as shown in Fig. 1. Additionally, for a conventional skin-stringer-frame built-up panel, the frame shear clip is typically discontinuous to allow the stringer to pass through the frame. If such an arrangement were used for the HWB, the frame would be less effective in bending and axial loading than a continuous frame that is attached directly to the skin, ultimately resulting in a heavier panel.

To overcome these challenges, an improved fuselage panel should be designed as a bi-directionally stiffened panel, where the wing bending loads are carried by the frame members and the fuselage bending loads are carried by the stringers. The panel design should also include continuous load paths in both directions, stringer and frame laminates that are highly tailored, thin skins designed to operate well into the post-buckled design regime, and with crack-arresting features designed to minimize damage propagation. These features are necessary to overcome the inherent weight penalties of the non-circular pressure cabin.

III. PRSEUS Concept

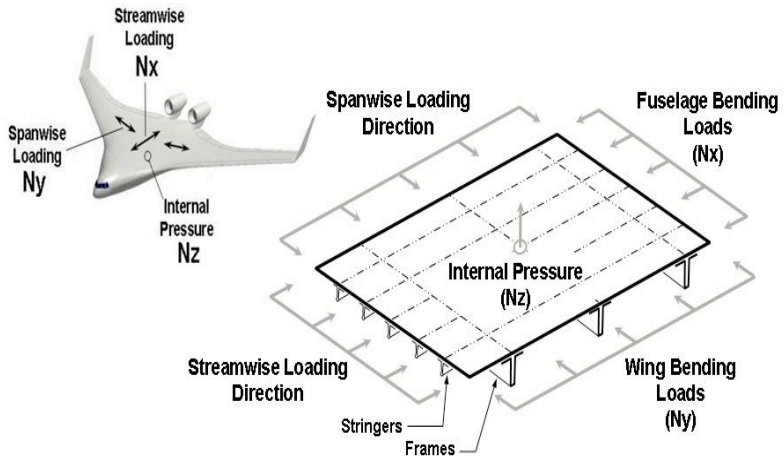

Figure 1. Combined loading on a HWB pressure cabin.

The PRSEUS design-and-fabrication approach incorporates damage arrestment, improved load paths, and weight-reducing design features, which results in a highly efficient structural concept. It is a conscious progression away from conventional laminated and bonded methods of assembly, and has evolved to become a one piece co-cured panel design with seamless transitions and damage-arrest interfaces. The highly integrated nature of the PRSEUS stiffened panel design is enabled by the use of through-the-thickness stitching, which ultimately leads to unprecedented levels of fiber tailoring and structural optimization potential.

The PRSEUS panel concept is a combination of dry carbon warp-knit

fabric, pultruded rods, foam core, and stitching threads. The fabric consists of AS4 carbon fiber layers with a (44/44/12) fiber architecture, where the values are percentages of (0/±45/90) degree plies. Each stack has a nominal cured thickness of 0.052 inches. Multiple stacks of the warp-knit material can be used to build up the desired part stiffness, strength, and configuration. These materials are brought together in a unique manner to create a stiffened panel geometry that utilizes resin infusion and out-of-autoclave curing to reduce recurring fabrication costs and allow the construction of very large panels. The resulting panels are one-piece unitized assemblies with a highly integrated, stiffened-panel design enabled by the use of through-the-thickness stitching, which ultimately leads to unprecedented levels of fiber tailoring and load-path continuity between the individual structural elements.

Structural continuity is maintained by eliminating mechanical attachments, gaps, and mouse holes to provide uninterrupted load paths between the skin, stringer, and frame elements, as shown in Fig. 2. The stringer contains a pre-cured high-stiffness pultruded rod, made of Toray unidirectional T800 fibers with a 3900-2B resin above a thin web, with the flanges stitched to the skin. Stacks of fabric are used for all webs, flanges, tear straps, and the skin. Foam-filled frames are perpendicular to the stringers and also have flanges which are stitched to the skin. Load-path continuity at the stringer frame intersection is maintained in both directions by passing the rod-stringer through a small keyhole in the frame web. The 0-degree fiber dominated pultruded rod increases local strength and stability of the stringer section while simultaneously shifting the neutral axis away from the skin to further enhance the overall panel-bending capability. Frames are placed directly on the inner moldline skin surface, and are designed to take advantage of carbon fiber tailoring by placing bending and shear-conducive lay ups where they are most effective. By shifting the neutral axis away from the skin, this design creates efficient load paths in both directions that are beneficial to the stability and bending resistance of the panel. Vectran threads are used to stitch the stiffeners to the skin and at other discontinuities. Since all the interfaces are stitched together to provide through-the-thickness strength, a high degree of fiber tailoring is possible even with layered composite material systems, which are known to be brittle and prone to delamination. Extra thickness in the skin and flanges is not needed to resist out-of-plane motion.

The stitching is also used to suppress out-of-plane failure modes. Suppressing these failure modes enables a higher degree of tailoring than would be possible using conventional laminated materials. Stitching arrests cracks and controls damage propagation within a layered material system. By strategically placing stitch rows along the key structural interfaces, traditional resin-dominated failure modes can be suppressed, so that the optimum strength of the panel can be more nearly realized. Using through-the-thickness stitching to locally reinforce the out-of-plane-direction interfaces not only makes integral construction possible, but also enables a new type of damage arrest and fail-safe redundancy into the structure that was previously reserved for ductile materials and not normally associated with brittle composite systems.[15,16]

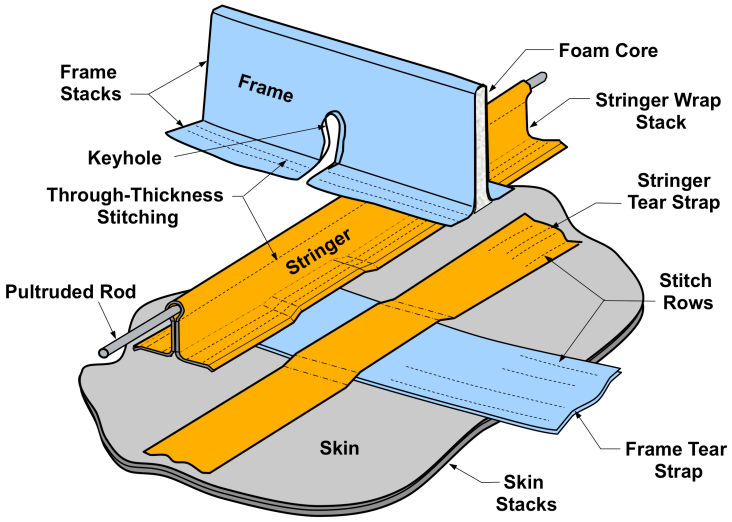

Figure 2. Exploded view of a PRSEUS concept.

The resulting bi-directionally stiffened panel design is ideal for the HWB pressure cabin because the design is highly efficient in all three loading directions, and the stitching on the panel reacts pull-off loading and increases panel survivability. These features are also applicable to barrel-fuselage sections with thin skins and for wing structures to improve structural efficiency and reduce weight. This approach would allow thin fuselage skins to safely buckle. It also allows the stringer to pass through fuselage frames and wing rib and spar caps.

IV. PRSEUS Development

A series of building block tests were conducted to explore the fundamental assumptions related to the capability and advantages of PRSEUS panels. The building block tests addressed tension,[5,12] compression,[5,6,8,11] and

pressure[5,12,13] loading cases of the HWB pressure cabin as illustrated in Fig. 3. The emphasis of the development work has been to assess the loading capability, damage arrestment features, repairability, post-buckling behavior, and response of flat panels to out-of-plane pressure loading. Each building block test was accompanied by analysis for prediction and post-test comparisons. All test articles were fabricated at the Boeing stitching center in Huntington Beach, CA. The design, analysis, and testing activities were divided between NASA and Boeing. This series of tests, with their corresponding analyses, have demonstrated that PRSEUS panels are capable of meeting the unique tension, compression, and pressure loading conditions of a HWB pressure cabin leading up to the final complex built-up structure.

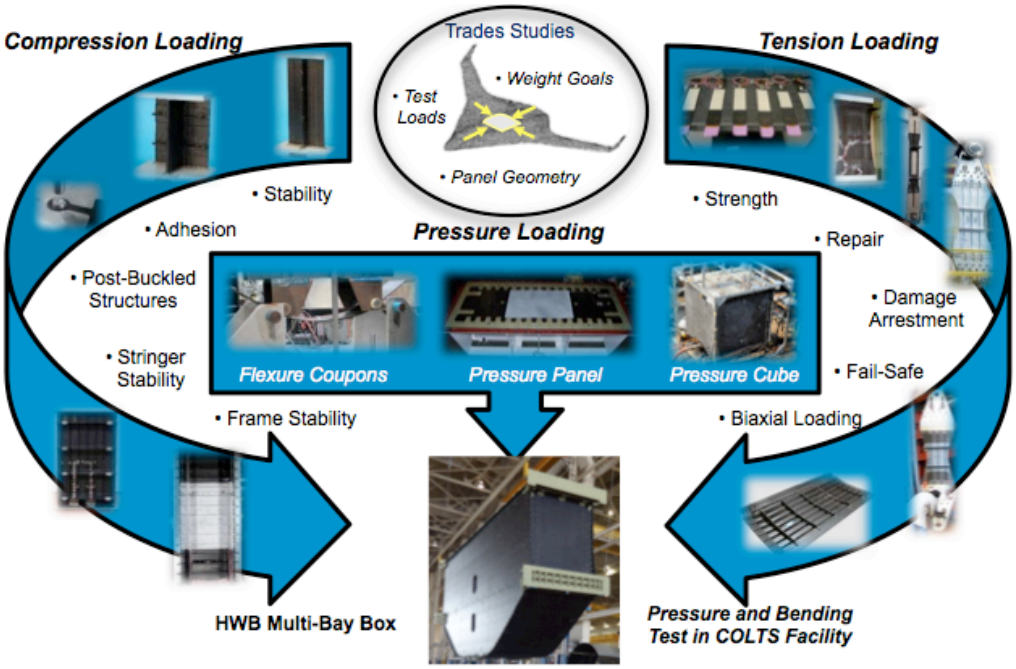

Figure 3. Development path leading to a HWB large-scale test article.

V. MBB Test Article

The knowledge gained from the earlier steps of the building block development program was used to develop a large-scale MBB test article. This test article was the last step in the building block process for the HWB center fuselage section.

Developing the manufacturing process to build large unitized stitched panels was necessary to apply this technology to large commercial transport aircraft. This unitization is enabled by the use of dry material forms, single-sided stitching, and the unique self-supporting preform design that is used to eliminate internal moldline cure tooling. Using these technologies, complicated stitched preforms can be fabricated without exacting tolerances, and then accurately net molded in a single oven-cure operation using high precision outer moldline (OML) tooling. Since all of the materials in the stitched assembly are dry, there are no out-time limitations as with prepreg systems, which can restrict the size of an assembly because the assembly must be cured within a time-limited processing envelope. Additionally, the infusion and cure processes for PRSEUS panels require high temperatures, but only vacuum pressure, which eliminates the need for an autoclave and the limitations based on the size of the autoclave.

Hexcel HexFlow VRM 34 resin infusion is accomplished using a soft-tooled fabrication scheme where the bagging film conforms to the inner moldline surface of the preform geometry and seals against a rigid OML tool. The success of this approach has been demonstrated on PRSEUS panels up to 30 feet long, as shown in Fig. 4. This panel contains rod-stiffened stringers, foam-filled frames, and integral caps. Integral caps are similar to the foam-filled frames in that the stringers pass through the integral caps at keyholes, but the integral caps are solid laminates that only occur at locations where one panel joins to another. All elements are stitched together with no need for fasteners or fittings within the panel. The design and fabrication of this test article is described in Ref. 17-20.

Figure 4. Components of a PRSEUS panel.

The MBB test article was an 80%-scale component representing a section of the most heavily loaded portion of the HWB center section. The MBB consists of 11 PRSEUS panels that form the exterior shell and floor members, along with four interior sandwich rib panels that were used to divide the box width into thirds, as shown in Fig. 5. In a HWB aircraft, the bulkheads would be near the cockpit and near the tail. In the test article, they are only 7 feet apart, but they support the same type of loading as would be found in the actual aircraft. The panels used in the MBB are shown in Fig. 6.

The multi-bay pressure box was assembled at the Boeing C-17 assembly site in Long Beach, CA. A photograph of the completed multi-bay pressure box is shown in Fig. 7. Load-introduction hardware elements, identified as adaptor boxes in Fig. 5, and seen as the green elements on the sides in Fig. 7, were added to the test article to mate with the platens in the test facility, and ensure that the load was imparted to the test article in such a way as to avoid failure at these outer rib locations. After installation on the test article, these adaptor boxes were milled flat, so as to have the upper and lower boxes be coplanar on each side. Additionally, they were milled such that the planes would be parallel to each other to ensure seamless mating to the platens in the test facility. A detailed description of this procedure is given in Ref. 20. Prior to delivery to NASA, the interior and exterior of the test article were painted white to improve the visibility of cracks and delaminations that could form during testing. A graphic and photograph of the test article in the test facility are shown in Fig. 8.

Linear and nonlinear finite element analyses were performed to validate the design of the MBB and predict the behavior of the MBB under five critical load cases.[21,22] These loading cases were 1) an internal pressure load only, where the maximum load was 18.4 psi; 2) a load simulating a 2.5-g wing up-bending load case which subjects the crown panel to compressive loads; 3) a –1-g wing down-bending load case which subjects the crown panel to tensile loads; 4) a combination of pressure and down-bending; and 5) a combination of pressure and up-bending.

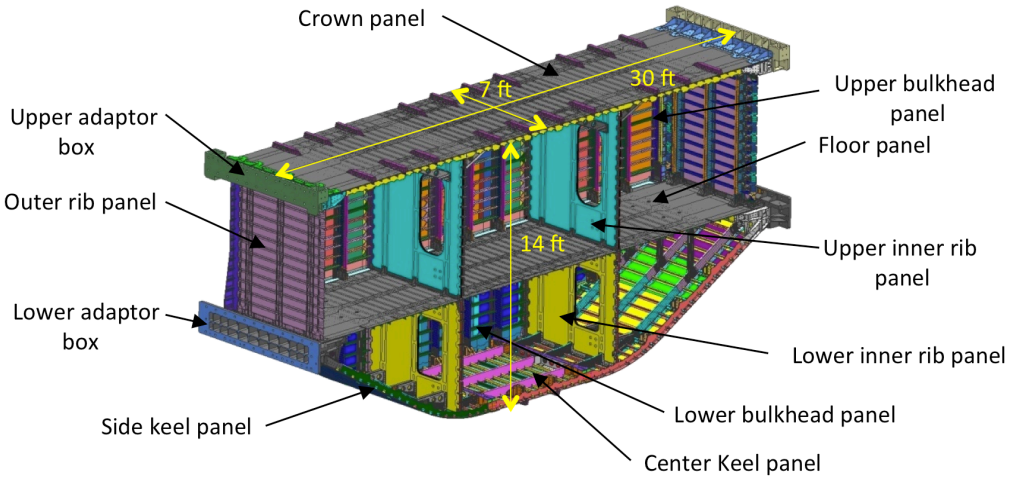

Figure 5. Components of the MBB.

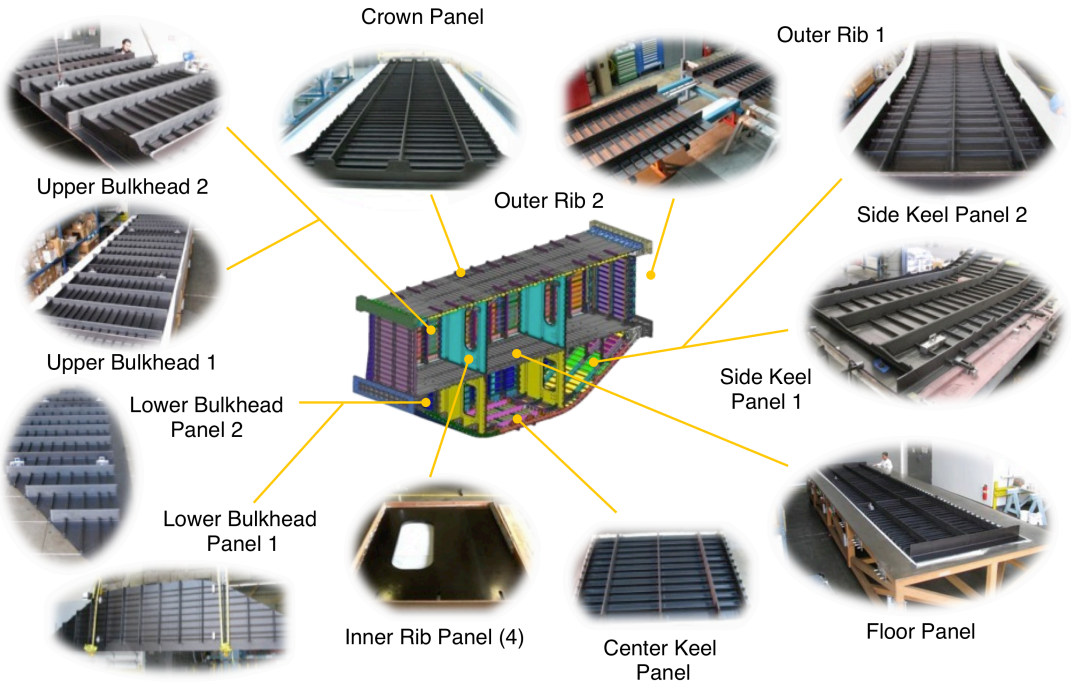

Figure 6. Composite panels in the MBB.

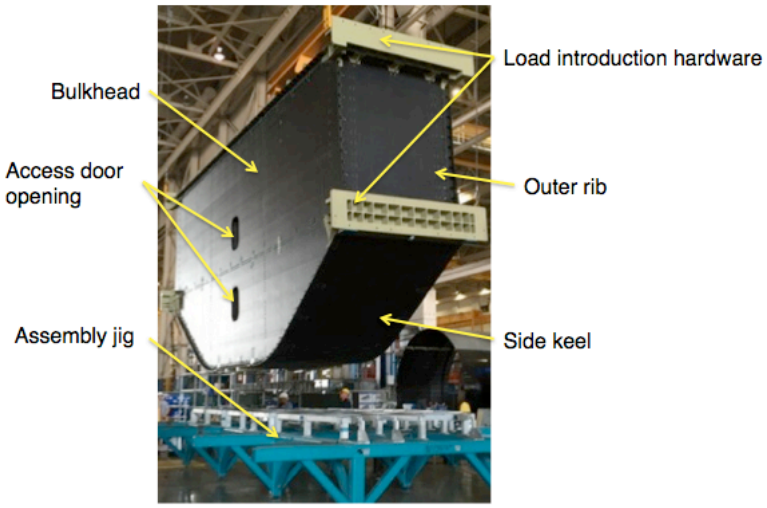

Figure 7. Fully assembled MBB.

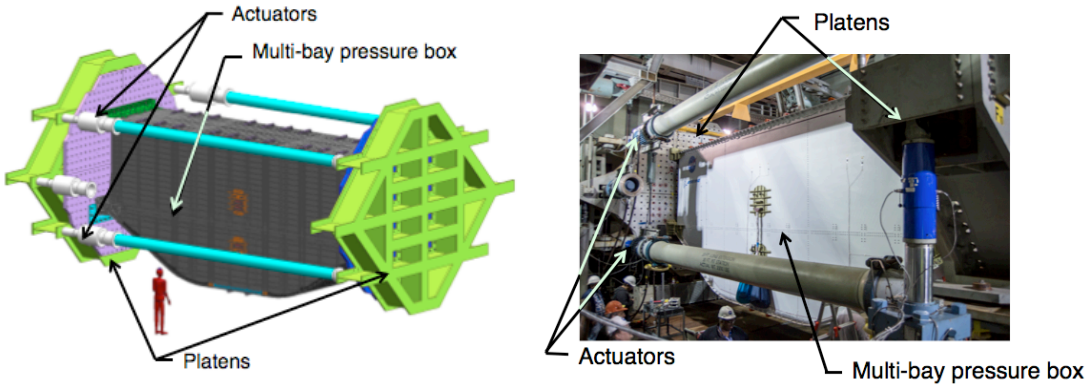

Figure 8. Test article between platens in the test facility.

VI. MBB Experimental Approach

The MBB was subjected to a series of loadings in the Combined Loads Test System (COLTS) Facility[23-25] at NASA Langley Research Center. Testing was conducted with the structure in the pristine condition, with intentional minor damage, and with intentional severe damage.

A. Instrumentation

Several types of instrumentation were used to monitor and record data during each test. There were 480 unidirectional and 36 rosette strain gauges, 15 linear variable displacement transducers (LVDTs), four pressure transducers, four fiber optic wires, four digital video image correlation (VIC) systems, 26 acoustic emission sensors, and nine video cameras used to record the behavior of the test article and the COLTS system. Data from the strain gauges, video digital image correlation systems are presented herein. Additional results are presented in References 13, 14, 26-29.

Plots of critical strain gauges and LVDTs were monitored during each test to track the structural behavior in real time, to compare to predictions, and to evaluate the operation of the loading system. Selected full-field displacements and strains were also monitored. Data from the strain gauges, transducers, and load cells were recorded at a rate of 10 scans per second and from the VIC system once every 5 seconds. Strain gauges were applied to every panel, but full-field monitoring was only used on the aft bulkhead, the crown, and the center keel. For these areas, a speckle pattern, consisting of black paint dots on a white-paint background, was applied to a portion of the test article, as shown in Fig. 9. Two still-image cameras were positioned to view each speckled region to simultaneously photograph the pattern. These images were compared to determine the displacements in the x-, y-, and z-directions and the in-plane strains. The methodology for using the photographs to determine displacements and strains is presented in Ref. 30.

B. Load Sequence and Control

The MBB was tested in three conditions. First, the test article was subjected to loads up to design ultimate load (DUL) in all five load cases. Second, barely visible impact damage (BVID) was inflicted to the center keel and one upper bulkhead and the test article was again subjected to loads up to DUL in all five load cases and then to loading 10% greater than DUL in the up-bending and up-bending plus pressure load cases. Finally, discrete source damage (DSD) in the form of a severed frame was inflicted on the test article and loading in the up-bending case was conducted to failure.

Mechanical loads were applied to the test article to simulate critical flight conditions and internal pressure loads were applied to represent cabin pressure. During testing, mechanical loads were applied alone, pressure was applied alone, and combinations of internal pressure and mechanical loads were applied. In each case, loading was quasi-static and slow enough to ensure that the actuators stayed synchronized with each other and with the pressure load. The mechanical loads were applied to the test article through four actuators, located at the four corners of the test article, which were used to rotate the platens relative to each other. Internal pressure was introduced into the test article through a valve in an upper bulkhead panel access door to simulate cabin pressure. Holes in the floor ensured

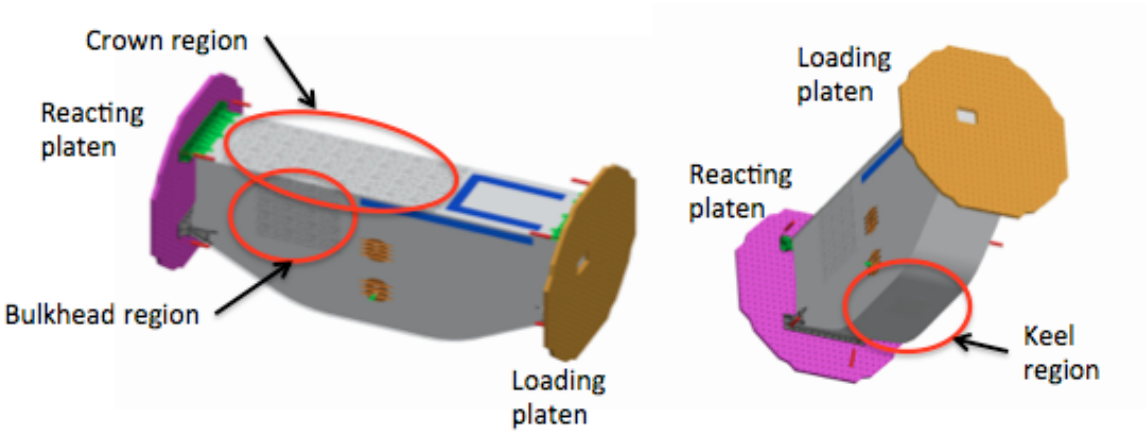

Figure 9. Digital video image correlation regions.

that the pressure remained constant in the upper and lower sections of the test article. Design limit load (DLL) for pressure was determined based on the intended cruise altitude and was assumed to be 9.2 psi. DUL for the pressure-only case was determined to be 18.4 psi. During combination load cases, a pressure load of 13.8 psi was applied.

When mechanical loading is applied in COLTS, both platens rotate around their center of gravity, but only the "loading" platen translates. This behavior means that the platen displacements caused by the rotation of the "reacting" platen are not the same as the displacements caused by the rotation and translation of the loading platen. Each actuator applies a load and displacement; but since each actuator is connected to both platens, the relative motion is controlled, even though the individual motion of the platens is not.

Although the applied actuator loads or applied displacement were nominally identical in magnitude, the lower actuators operated in the opposite direction compared to the upper actuators; therefore, when the load in the upper actuators was positive, the load in the lower actuators was negative. This connection was accomplished by slaving all actuators to a single actuator and controlling the load or displacement in that actuator.

In all loadings to DUL or less, when pressure loading was applied simultaneously with the mechanical load, the pressure load and actuator load were programmed to ramp together from zero to maximum loading. When mechanical loading greater than DUL was applied, pressure ramped with the mechanical load, but was programmed to not exceed the DUL condition for pressure. In each test, loads were ramped from zero to the maximum load with short pauses to compare test data to predictions.

The pristine and impact-damaged test article loadings were conducted using load control while the DSD testing was conducted using a combination of load and displacement control. Actuator load as a function of time is shown in Fig. 10 for the pristine DUL up-bending load case to demonstrate the accuracy of the control system in controlling the applied actuator loads. Load magnitudes for the four active actuators stayed in excellent agreement with each other throughout the test. This level of synchronization of the actuators was typical of the loading in all tests conducted under load-control. The test sequence is shown in Table 1. The –1-g DUL level corresponds to actuator loads of 95.4 kips. The 2.5-g DUL level corresponds to actuator loads of 238.5 kips.

The last loading of the BVID structure applied two load cases. The load sequence for the test to loading greater than DUL is shown in Fig. 11. In this test, first the load was ramped to DUL in the up-bending plus pressure condition, represented by the red line in the figure. Then, the pressure was held constant while the mechanical load was increased by 10%. Then, the mechanical load was decreased to DUL. The purple line in the figure represents the pressure-hold sections of the loading. Then, the mechanical load was held constant while the pressure load was removed, leaving the test article at DUL in the up-bending condition without pressure. This portion of the load sequence is represented by the blue line. Then, the mechanical load was increased to 10% greater than DUL, and held briefly. This portion of the load sequence is represented by the green line. Finally, the mechanical load was removed.

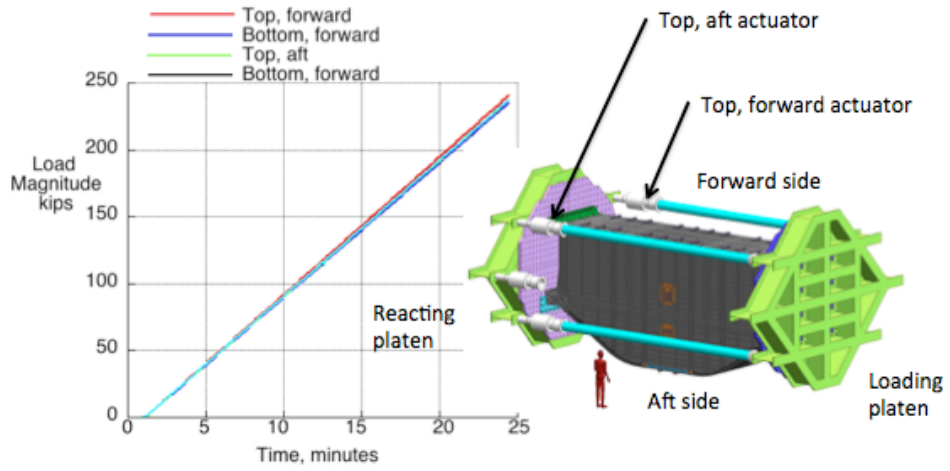

Figure 10. Actuator applied loads for up-bendng to DUL case for pristine test article.

Table 1 Applied Load for DUL Tests

	Mechanical load (% of DUL)	Pressure (% of DUL)
Pristine		
Down-bending	100	0
Down-bending plus pressure	100	75
Up-bending	100	0
Up-bending plus pressure	100	75
Pressure only	0	100
BVID		
Down-bending	100	0
Down-bending plus pressure	100	75
Pressure only	0	100
Up-bending	100	0
Up-bending plus pressure	100	75
Up-bending plus pressure	110	75
Up-bending	110	0
DSD		
Up-bending	101	0

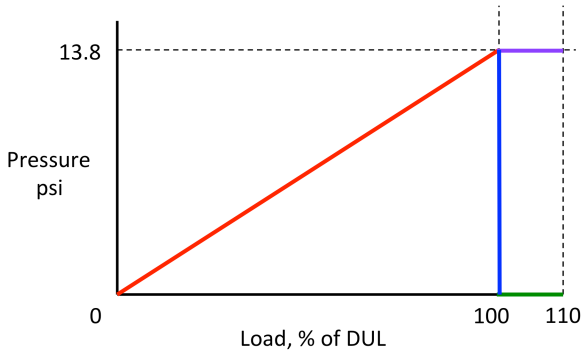

Figure 11. Loading to 110 % DUL.

For the DSD test, load control could have caused severe damage to the test article in the event of a catastrophic failure as the control system would have continued to apply load after the test article could no longer sustain load. Therefore, the top forward actuator was operated in displacement control where the applied actuator displacement was based on data acquired from testing of the undamaged structure. Since the DSD test was intended to fail the test article, the programmed maximum displacement value was not critical; however, the displacement rate was important and was selected to be consistent with the displacement

rate in prior tests. The displacement of the top aft actuator was programmed to be identical to that of the top forward actuator. Since all earlier tests were conducted in load control and comparisons were based on load, the bottom actuators were each programmed to have the same load magnitude as the actuator above them. Actuator load and displacement as a function of time are shown in Fig. 12 for the DSD test. The displacement of the top aft actuators is indistunguishable from the displacement of the top forward actuator. The load in the bottom forward actuator is indistinuishable from the load in the bottom forward actuator. This is consistent with the programming of the control system. However, the load distribution forward-aft was not identical and the displacements top-bottom were not the same. These differences can be attributed to the fact that the location that the platens rotated around was not at the vertical center of the test article. With DSD, the load that would have gone into the center frame was forced into the outer frames in the crown. The load distribution was influenced by the cutouts in the inner ribs, which were on the forward side of the inner ribs.

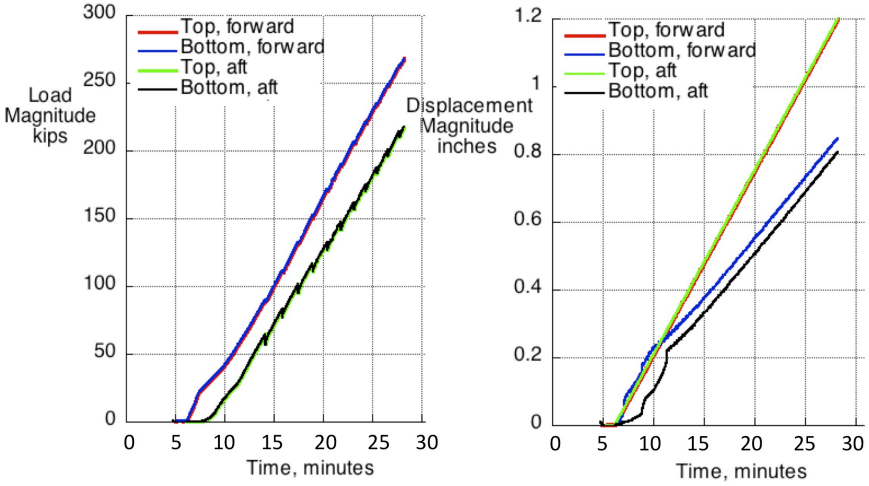

Figure 12. Actuator load and displacement during the DSD test.

C. Damage Application

After the completion of the pristine structure tests, BVID was inflicted to the forward upper bulkhead and center keel panels. Three impacts to the interior of the structure, on the stiffened side of the upper bulkhead, and three impacts to the exterior of the structure, on the unstiffened side of center keel, were inflicted. Damage to the interior was inflicted using a spring-loaded impactor. Interior impacts were intended to represent a range of locations and the type of damage possible due to service events such as tool drops. Damage to the exterior was inflicted using a gravity-fed apparatus. Exterior impacts were inflicted to an area of the structure that would buckle during loading to evaluate whether typical exterior impacts caused by runway stones, service vehicles, etc., would degrade the post-buckling performance of the structure. In each case, a weight with a one-inch-diameter hemispherical tup was used for the impact. A detailed description of the impact method and results is presented in Ref. 31.

BVID for the interior sites corresponds to 20 ft-lb for the top of the stiffeners, which causes little damage, but is the maximum energy required for internal impacts for commercial aircraft, and 15 ft-lb for the skin mid-bay location, which yields visible damage that is evident. Damage was inflicted at locations at the top of a stringer, at the top of a frame, and at a mid-bay location between stiffeners, as indicated in Fig. 13. BVID for the exterior sites corresponds to energy levels of 60 ft-lb, 50 ft-lb, and 15 ft-lb for the frame flange, the stringer flange and the mid-bay locations, respectively. Damage was inflicted at these locations as indicated in Fig. 14. In Fig. 13 and Fig. 14, the impact sites are indicated by a circle, square, and triangle on the photograph, representing the frame, mid-bay, and stringer impact locations, respectively. A sketch of the location for the exterior impacts relative to the stiffener flange is shown in Fig. 15.

One of the exterior impacts was inflicted slightly away from the planned impact site. This impact was to the thin-skin region instead of at the adjacent flange. Therefore, the damage was more severe than intended. The damage was clearly visible from the exterior and interior and, in fact, a through-hole was created. Evaluation of the damage at this location relative to the anticipated loading and stress state indicated that this damage would not reduce the ability of the structure to sustain mechanical load, but could reduce the ability of the structure to support internal pressure loads. Therefore, a non-structural patch was taped over the hole on the stiffened side of the center keel. Ultrasonic scans were conducted immediately before and immediately after the impacts, so that the extent of damage caused by the impacts could be quantified. These scans indicated that delamination occurred at the keel skin and flange impact sites, but was arrested at the closest stitch line to the impact site. Scans of the bulkhead stiffener impacts found no damage. Scans of the skin interior impact showed delamination from the impact site to the closest stitch line to the impact site, which was at the adjacent flange edges. Ultrasonic results are discussed in Ref. 32 and 33.

Figure 13. Impact sites on the upper bulkhead.

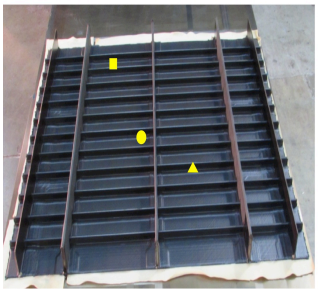

Figure 14. Impact sites on the center keel.

VII. Results and Discussion

The results presented herein focus on the DUL tests since the tests to lesser loads generally did not demonstrate any significant behavioral difference from the DUL tests. Results are shown first for the pristine structure and then selected results are shown for the BVID and DSD tests. For pristine tests, full-field displacement results at DUL and at selected load levels are shown; then, strain gauge results are shown; and finally, full-field strain results at DUL are shown. The full-field displacement and strain gauge results presented herein include only selected locations where large strains and nonlinear strains occur. For BVID and DSD tests, only strain gauge results are shown.

A. Displacements

Full-field out-of-plane displacements for a portion of the crown, aft bulkhead, and keel are shown in Fig. 16-20 at DUL. Only selected full-field images shown herein whereas all the images from the VIC regions are shown in Ref. 13. Displacements are shown for the down-bending and down-bending plus pressure cases in Fig. 16 and 17, for the up-bending and up-bending plus pressure load cases in Fig. 18 and 19, and for the pressure-only load case in Fig. 20. In all full-field displacement figures, positive displacements are outward from the plane of the panel. The white regions in each plot are areas where data could not be acquired due to features on the surface of the panels such as fittings, fasteners, strain gauges, and wires. The panels shown are those with the largest deformations and those demonstrating buckling behavior.

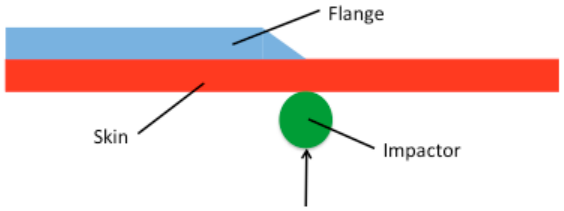

Figure 15. Exterior impact site near the flange.

These full-field images indicate that when mechanical load is applied, the skin of the panel in compression (crown for up-bending and keel for down-bending) buckles between the stiffeners. However, the results for the combined load cases show that the pressure loading has more influence on the crown and keel panels than the mechanical load. When pressure is applied, all panels bow outward. In the combined load cases, the deformation pattern is a combination of pressure pillowing and buckling. The largest displacement is in the pressure-only load case in the bulkhead panel. Small buckles occur between the stiffeners in the bulkhead panel in the up-bending load case. These buckles occur near the bulkhead-to-crown attachments and are caused by the shear loading in the bulkheads induced by the bending of the test article. While buckles in the crown and keel acquire an in-out pattern early in the test and retain that pattern, the buckle mode shape in the bulkheads changes with as loading is increased. The largest out-of-plane deformation is in the upper bulkhead in the pressure-only load case since that case applies the largest pressure load and the bulkhead has the largest distances between connections to other panels.

Deformation patterns for the bulkhead at the additional load levels of 60% and 90% DUL are shown in Fig. 21. This change in displacement pattern includes changes in the number of half-waves in the buckled region. Regardless of the cause or magnitude, these buckles occurred in DLL and DUL tests and did not appear to cause damage to the test article and did not compromise the ability of the test article to support DUL.

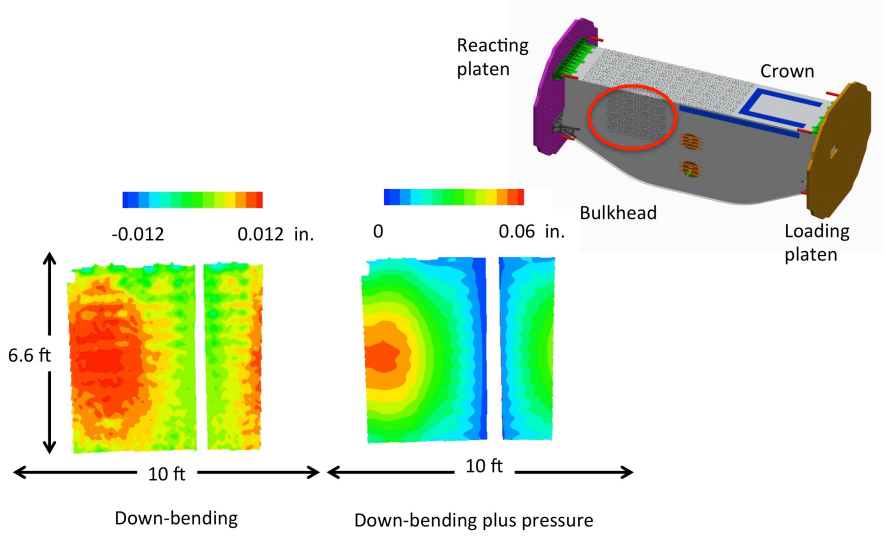

Figure 16. Bulkhead full-field out-of-plane displacements for the down-bending and down-bending plus pressure load cases.

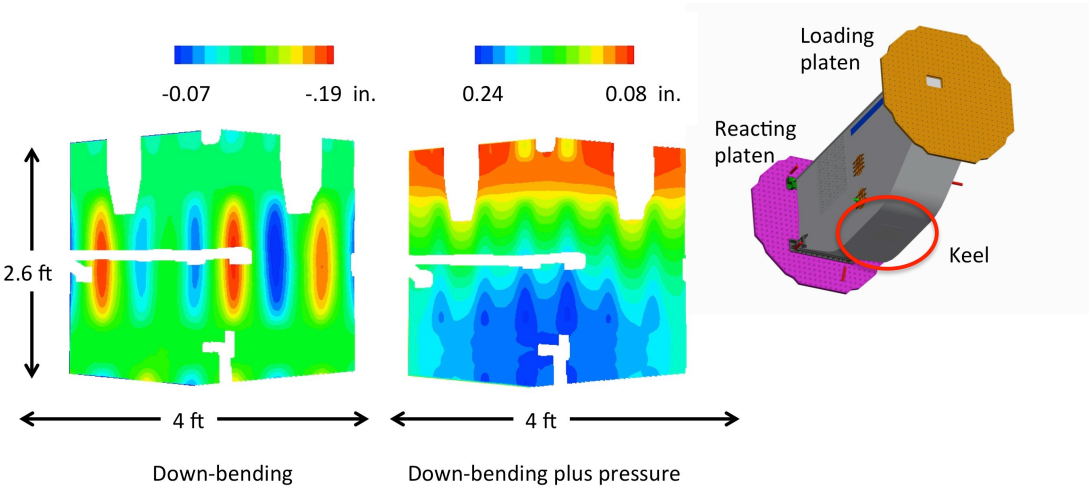

Figure 17. Center keel full-field out-of-plane displacements for the down-bending and down-bending plus pressure load cases.

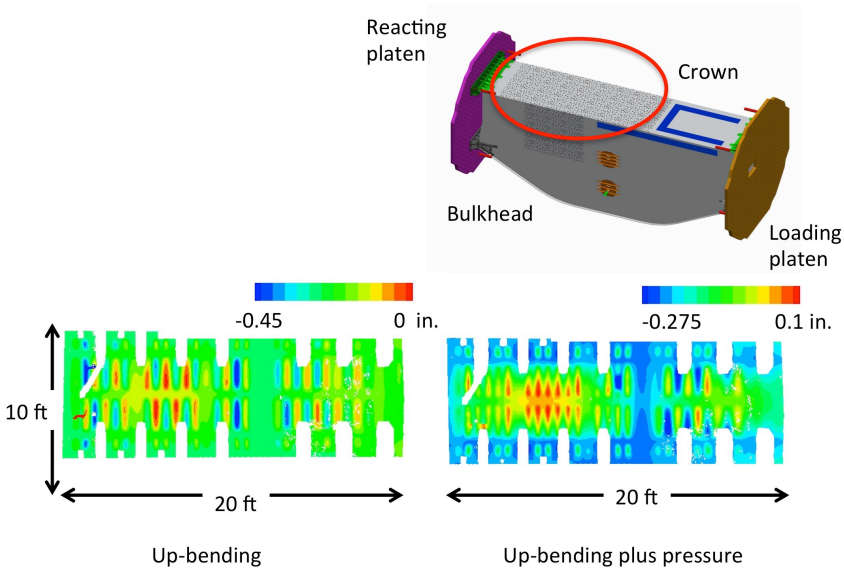

Figure 18. Crown full-field out-of-plane displacements for the up-bending and up-bending plus pressure load cases.

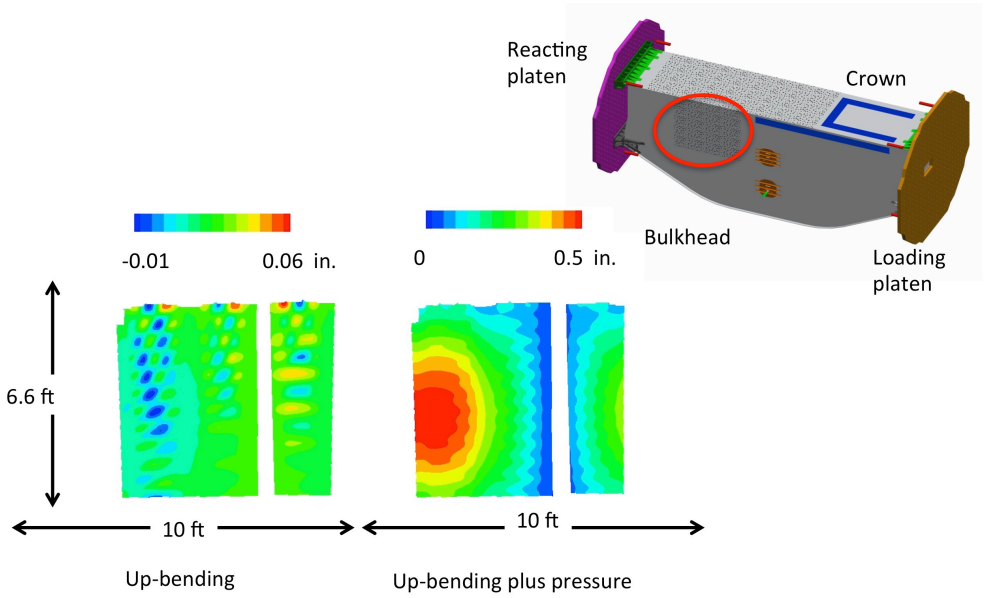

Figure 19. Bulkhead full-field out-of-plane displacements for the up-bending and up-bending plus pressure load cases.

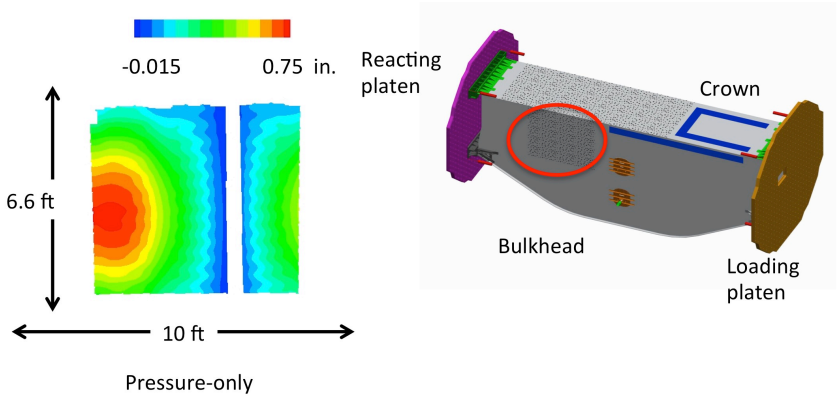

Figure 20. Bulkhead full-field out-of-plane displacements for the pressure-only load case.

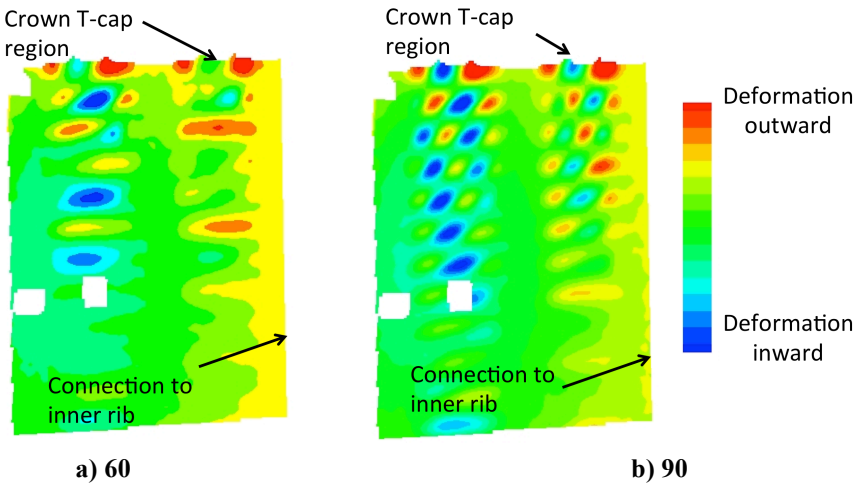

Figure 21. Bulkhead out-of-plane deformation pattern changes as the mechanical loading increases in up-bending load case (percentage of DUL).

B. Significant Strain Responses

Strain gauge results are grouped into plots based on the location and orientation of the gauges. In most cases, an inset image is included in the figure identifying the location of the gauge where boxes on the inset correspond to gauge locations on the sketch of the panel. These boxes represent either a single gauge or a back-to-back pair. When colored boxes (e.g. red, blue) are used in the inset image, the colors of the curves in the plot correspond to the strain gauge location shown on the inset. When grey boxes are used, typically one panel sketch is used to represent multiple symmetric locations on the test article and a legend is used to identify which panel or other specific location on the test article where the gauge is located. When mechanical load is present, the controlled actuator load is used for plotting; pressure is, therefore, only shown in the pressure-only load case.

1. Buckling

The down-bending load case applies tension to the crown panel, compression to the keel panels and floor, and shear load into the bulkheads. Strain gauges on the floor and on the center keel were located to capture behavior in the down-bending load case. Strains in the center keel skin at the mid-bay location in back-to-back pairs parallel to the frames capture local skin buckling behavior and are shown in Fig. 22. The strain on the unstiffened side of the panel is represented by solid curves, and the strain on the stiffened side of the panel is represented by dashed curves. The colored boxes on the inset image of the center keel panel shows the location of eight back-to-back pairs of strain gauges. These results indicate that each bay of the keel panel buckled between the stiffeners at a load of approximately 40 kips. By noting that some exterior gauges showed positive strain and some exterior gauges showed negative strain, some bays deformed inward and some bays deform outward. This finding is consistent with the full-field displacement results. The magnitude of the strains in the buckled regions never exceeded 0.002 in./in. This strain does did exceed the design strain values of 0.0059 in./in. in tension and –0.0048 in./in. in compression for notched or damaged structure and did not indicate any failures.

The up-bending load case applies a combination of compression and bending into the crown, shear load into the bulkheads, and tension loads into the keels. Strain gauges on the crown, center keel, side keels, and upper bulkheads were located to capture behavior in the up-bending load case. Strains in the crown skin at mid-bay location in back-to-back pairs parallel to the frames capture local skin buckling behavior and are shown in Fig. 23 and 24. The strain on the unstiffened side of the panel is represented by solid curves, and the strain on the stiffened side of the panel is represented by dashed curves. The colored boxes on the inset image of the crown show the location of four back-to-back pairs of strain gauges in Fig. 23 and 24. These results indicate that the crown panel skin began to deform out-of-plane immediately after loading began in most bays. By noting that some exterior gauges showed positive strain and some exterior gauges showed negative strain, it is clear that some bays deformed inward and some bays deform

outward. This finding is consistent with the full-field displacement results. Initial imperfections in the panel geometry may have influenced the deformation shape to determine which bays buckled in which direction. The mode shapes did not change through the course of loading. The magnitude of the strains in the buckled regions never exceeded the design strain values, the strains indicated no changes in buckle pattern, and no visible failures occurred at these sites.

Strain gauges were placed on the skin of upper bulkhead panel on the unstiffened (exterior) side near the connection to the crown panel in three quadrants of the test article (the fourth similar location was in the region where full-field data were acquired). Results for these strain gauges are shown in Fig. 25 and 26. These strain gauges were rosettes measuring strain parallel to the frame, perpendicular to the frame, and at a 45-degree angle to the frame. The colors of the curves on the plot correspond to the strain gauge locations shown in the inset image of the crown panel and the solid curves represent the locations toward the aft side of the test article. The long and short dashed curves represent the locations toward the forward side of the test article closer to the loading platen and the reacting platen, respectively. These measurements show that the largest magnitude of these strains is parallel to the frame and does not exceed 0.004 in./in. The abrupt change in slope in these strains as loading increased and the changes in VIC patterns indicates that the skin at these locations buckled, and that different bays changed mode shape at different load levels.

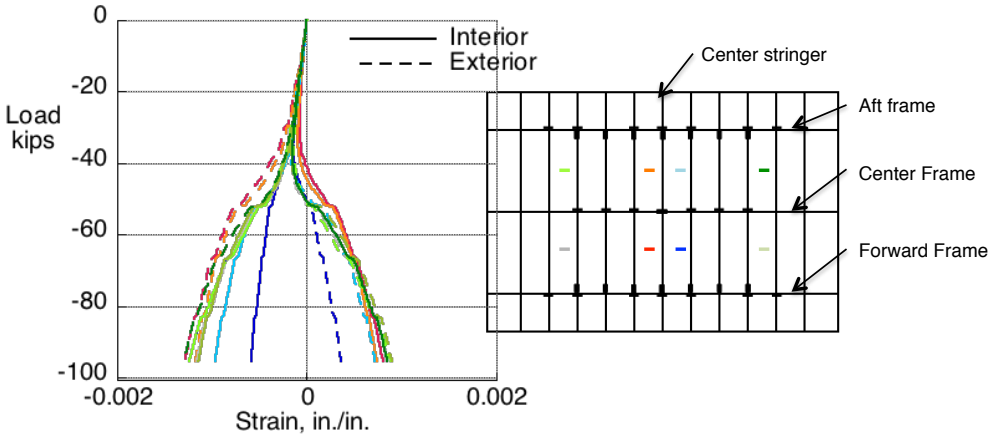

Figure 22. Strain in the center keel.

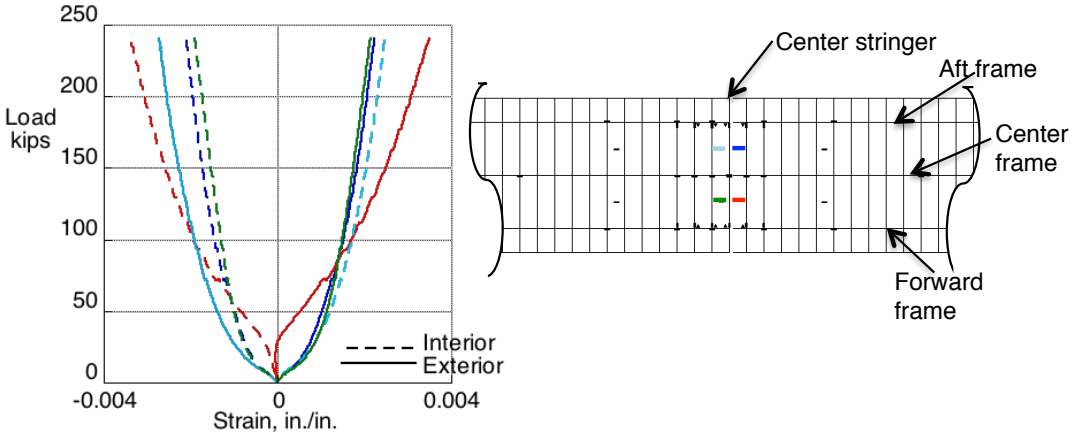

Figure 23. Strain in the crown skin at the back-to-back mid-bay gauges near the center stringer.

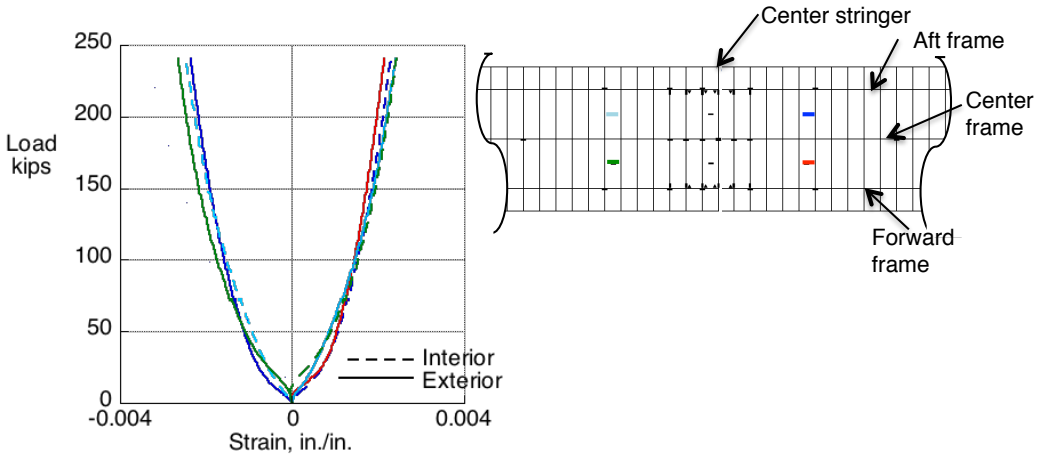

Figure 24. Strain in the crown skin at the back-to-back mid-bay gauges away from the center stringer.

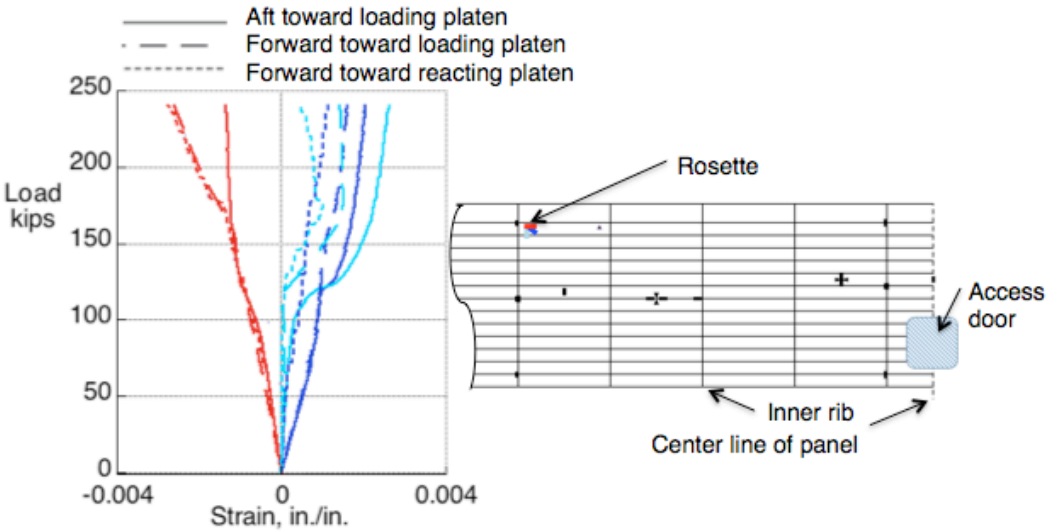

Figure 25. Strain on the exterior upper bulkhead skin from outboard strain rosettes.

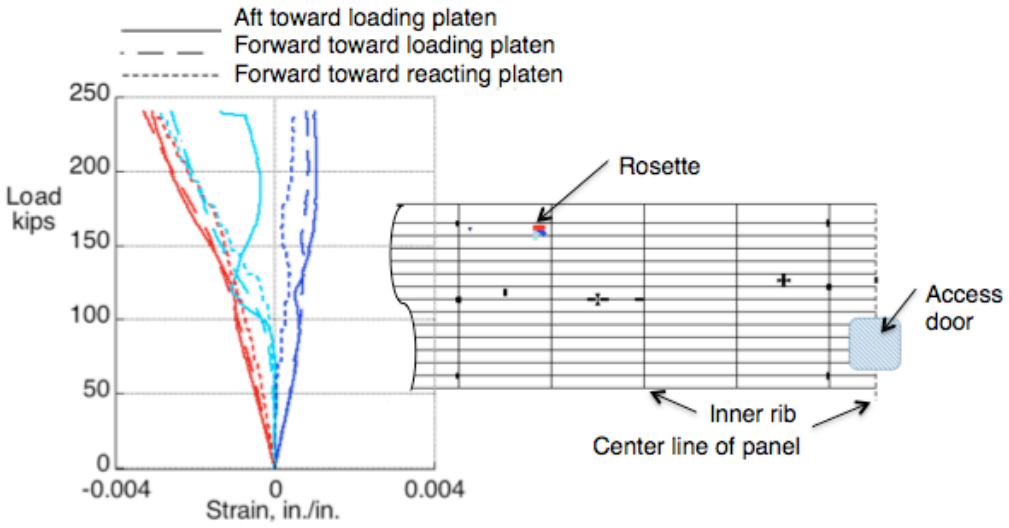

Figure 26. Strain on the exterior upper bulkhead skin from inboard strain rosettes.

2. Potentially High Strain Areas

In previous studies considering PRSEUS panels loaded in the frame direction, strain concentrations in the frame web near the keyhole contributed to panel failure.[7] To address that failure mode, additional stack material was placed in a cavity in the frame foam to reduce this concentration at the more highly loaded keyholes to prevent premature failure at this local feature.[21] To evaluate this design modification, strain gauges were placed on the center frame web approximately 0.3 inches away from the keyhole and parallel to the frame at critical frame-stringer intersections. The highest loading for the crown and keel frames was in the up-bending condition, placing the keyhole region in compression in the crown and tension in the keel. Results for seven critical keyholes for the crown center frame are shown in Fig. 27. Results for seven critical keyholes in the center keel in the center, forward, and aft frames are shown in Fig. 28a, 28b, and 28c, respectively. The keyhole strains did not exceed the design values in tension or compression. No damage was observed at these locations after the completeion of all DUL tests.

In previous studies considering PRSEUS panels under pressure, strain concentrations in the stringer near the keyhole approached the design value.[11] The largest strains in the stringers under the pressure loading would be near the center of the largest unsupported region. For the MBB, that location is in the upper bulkhead panels approximately half way between the floor and the crown and half way between the inner and outer ribs. Strain gauges were placed on the top of three stringers in the upper bulkhead panels, parallel to the rod and near the keyhole. The results for these gauges are shown in Fig. 29 for the pressure-only and up-bending plus pressure load cases. The gauge location is indicated by the gray box in the inset image, where only half of one bulkhead panel is shown since the other locations are symmetric in the other quadrants of the test article. The fourth strain gauge at these symmetric locations is not shown since that gauge stopped functioning early in the test sequence. The strains at the top of the stringer are linear throughout loading and do not exceed the design strain values. The strains for the pressure-only load case are slightly greater than the strains for the combined load case, indicating that the addition of the bending load slightly reduces the strain in the bulkhead stringers by preventing the bulkhead from bowing outward as much as when pressure is present.

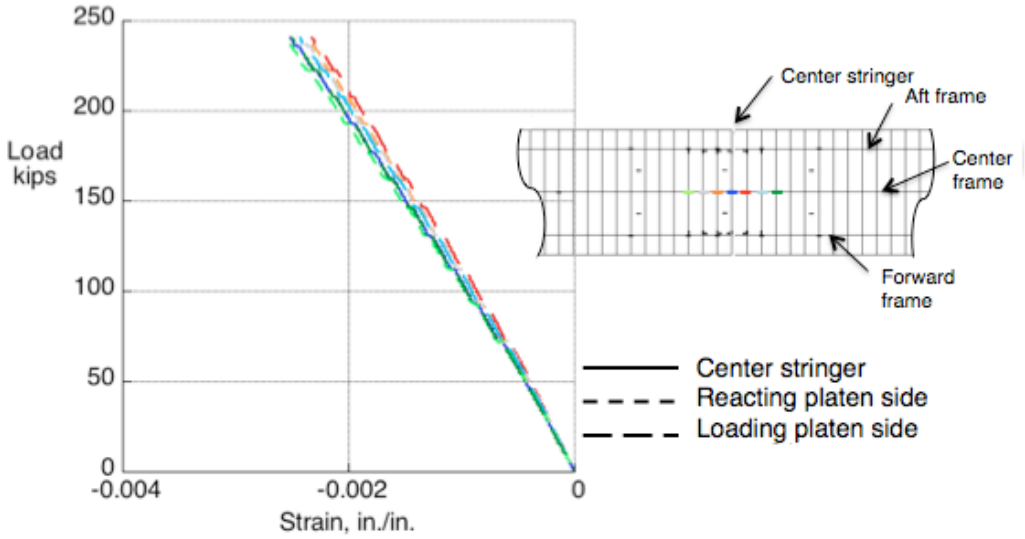

Figure 27. Strain in the crown center frame in a web above keyholes.

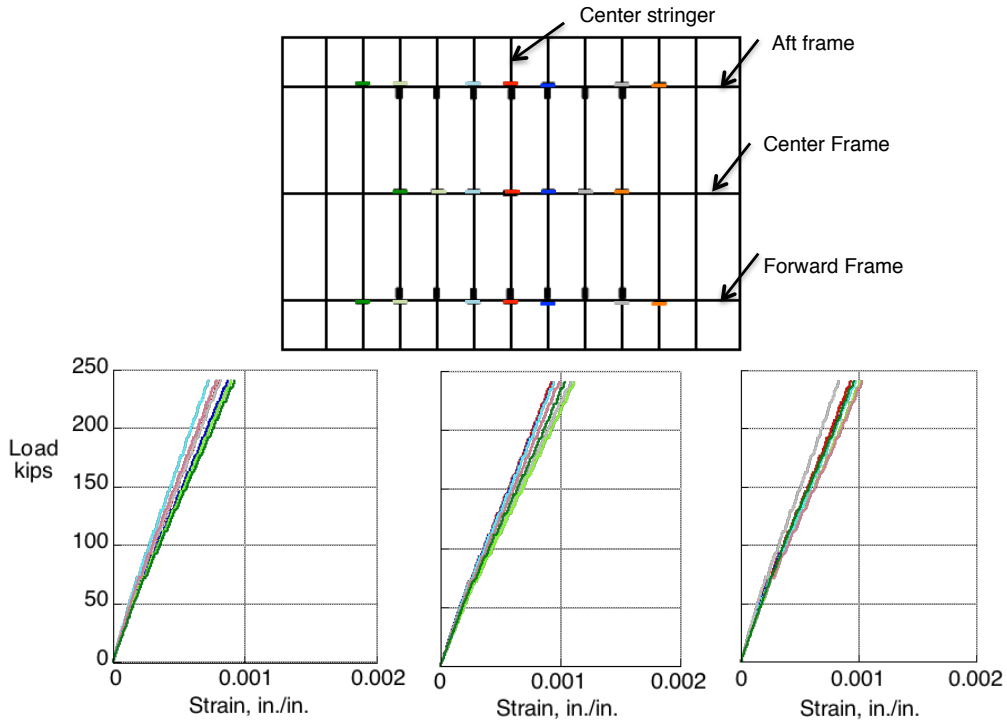

a) Center **b) Forward** **c) Aft**

Figure 28. Strain in the center keel frame webs above keyholes.

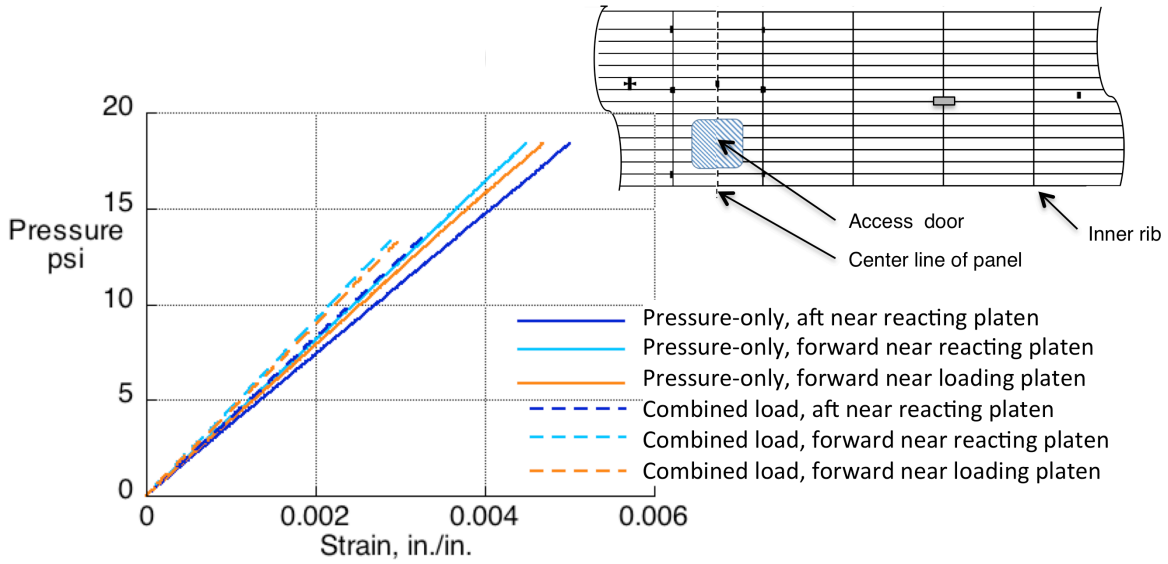

Figure 29. Strain in the top of the stringers of the upper bulkheads for up-bending plus pressure and pressure-only load cases.

Similarly, strains in the frames in the upper bulkhead panel can be significant when the panel bows outward during pressure loading. Strains at the top of the frames and on the external surface at the frame location in the upper bulkhead panels are shown in Fig. 30 at the locations indicated by the gray boxes in the inset sketch of an upper bulkhead panel. The results shown are for the pressure-only and up-bending plus pressure load cases. Strains on the unstiffened (exterior) surface are represented by solid curves and strains on the frames are represented by dashed curves. These strains do not exceed the design strain values. The strains for the pressure-only and combined load cases are indistinguishable, so the bending load does not contribute to the frame strain.

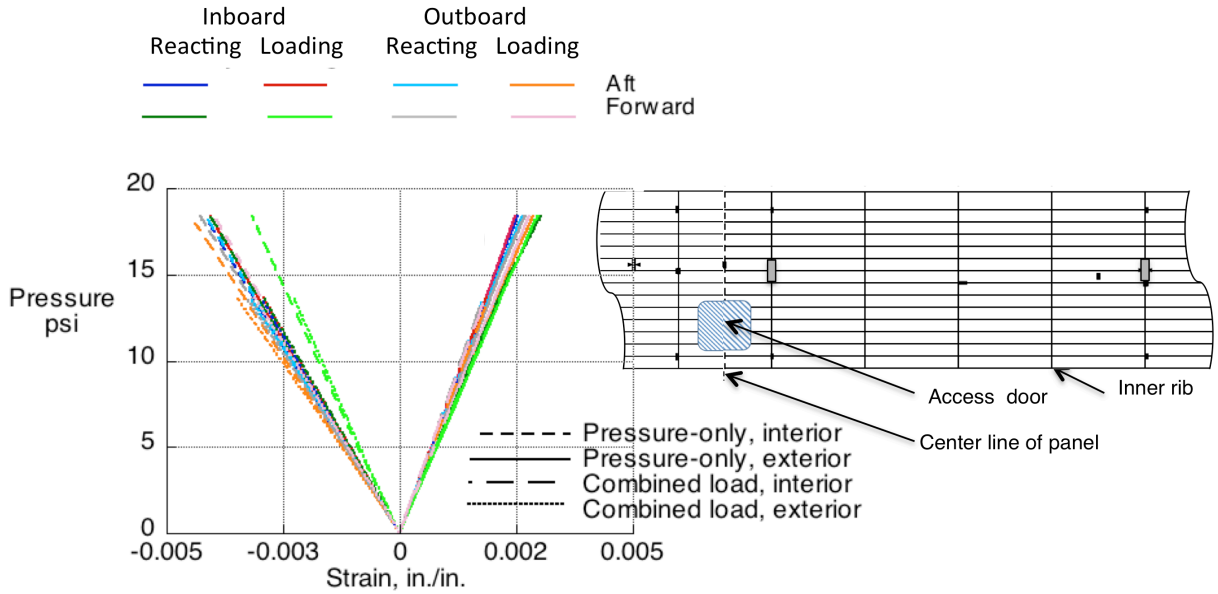

Figure 30. Strain in the top of the frames of the upper bulkhead for up-bending plus pressure and pressure-only load cases.

Pre-test analysis of the MBB indicated that there would be high strains in the crown panel skin on the stiffened (interior) side near the outer frame flanges and half-way between the stringers in the up-bending and up-bending plus pressure load cases.[22] These strains are shown in Fig. 31. These strain gauges were rosettes measuring strain parallel to the frame, perpendicular to the frame and at a 45-degree angle to the frame. The solid and short dashed curves represent the strains in the up-bending load case and the long dashed curves and the dotted curves represent the strains in the up-bending plus pressure load case. The strains in the combined-load case are slightly greater than the strains in the up-bending load case. Therefore, it is clear that the mechanical load influences these strains more than the pressure loading. These measurements show that the largest magnitude of these strains is parallel to the frame and does not exceed –0.006 in./in. This strain exceeds the design strain value of –0.0048 in./in. for damaged structure, but not the unnotched (pristine) value of –0.008 in./in.

A thorough visual examination of the test article was conducted after the completion of the pristine tests. Additionally, ultrasonic scans were completed at locations where high strain levels were found based on strain gage results and areas where pretest analysis inidicated damage could occur. No evidence of damage to the test article was found visually or by ultrasonic scans after the loading of the pristine test article.

C. BVID

After the pristine tests were completed, the test article was subjected to BVID. Strain gauges were added in the vicinity of each impact site and then the structure was again loaded to DUL in all five loading conditions. The impact damage had no effect on the global behavior of the test article. Strain gauges in the vicinity of the impact sites recorded strains with magnitudes less then 0.004 in./in. for all impact sites indicating that any increase in strain due to the impact did not exceed the allowable values slightly away from the impact site. Ultrasonic scans were conducted before and after loading and no apparent growth from the impact sites was detected.

The final BVID test subjected the test article to load greater than DUL in the up-bending and up-bending plus pressure load cases. In this case, the behavior of the crown and bulkhead are of interest. A behavior to consider is the strains in the crown skin at mid-bay locations, as shown in Fig. 32, using the same color scheme and curve type as described for Fig. 23. These results show that there is a change in buckle pattern early in the loading sequence, evidenced by the reversal in direction of the mid-bay back-to-back strain gauge results for the four mid-bay strain gauges closest to the center of the panel. After this reversal, strains increase in magnitude smoothly until the maximum mechanical load is reached, then decrease in magnitude as mechanical load is removed. Then, the strains change direction as pressure is removed. i.e., the tension surface goes into compression and the compression surface goes into tension. Finally, the strains increase again in magnitude, but at significantly less magnitude as the mechanical load is increased when no pressure is present. In order to clarify the behavior, consider the results using one back-to-back pair. The dark blue dashed and solid curves are an example of interior and exterior mid-bay strains.

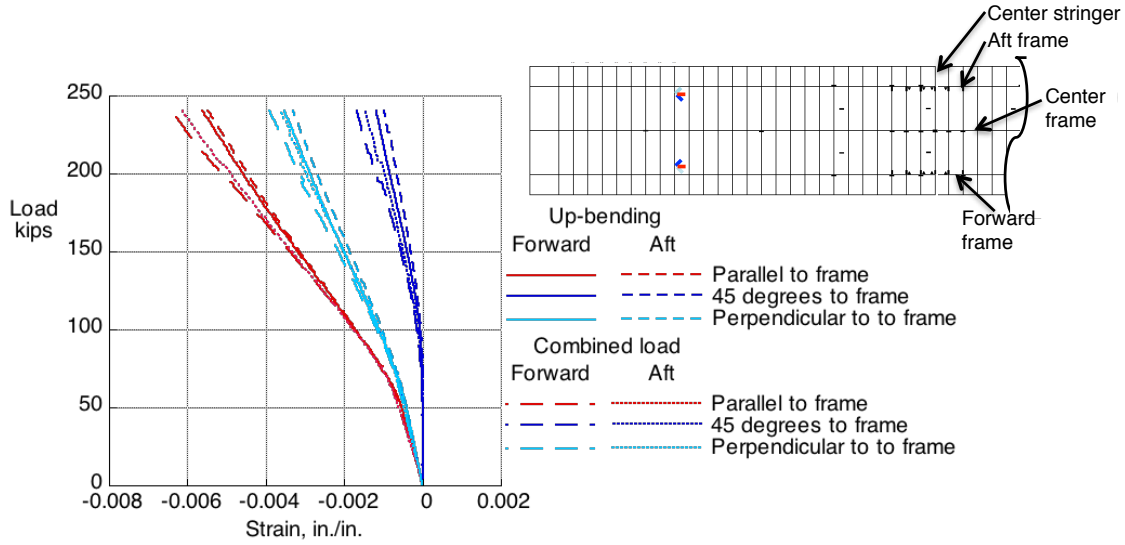

Figure 31. Strain in the strain rosettes on the interior of the crown in the up-bending plus pressure and pressure-only load cases.

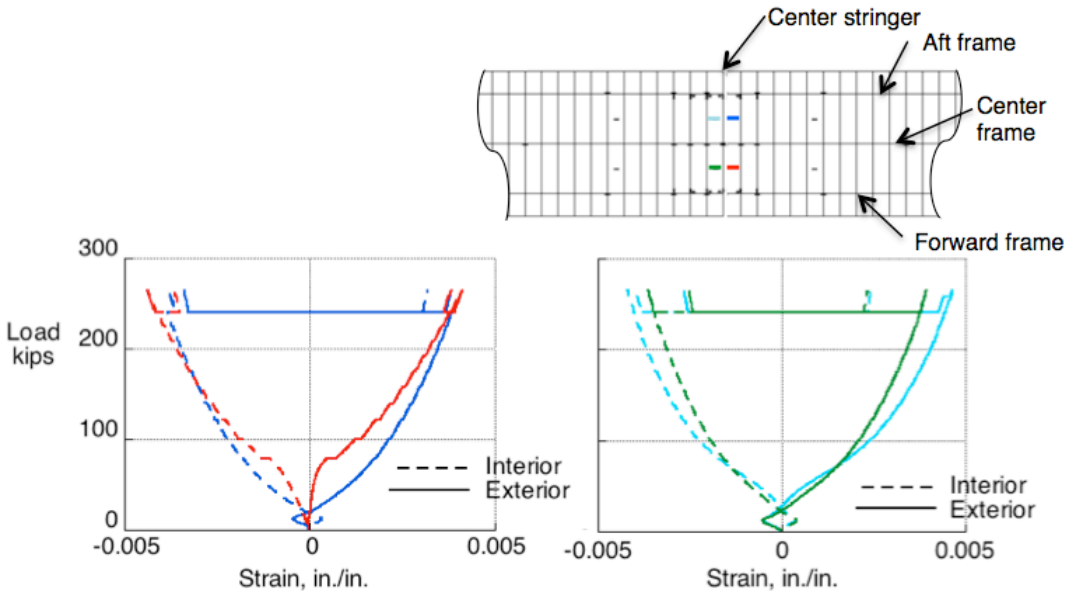

Figure 32. Strain in the crown skin in the load case to a load greater than DUL.

Each strain reverses direction at approximately 20 kips. Then, the strain magnitude increases smoothly until the maximum mechanical load is achieved, even though the pressure loading was not increased after 238 kips. At the maximum mechanical load, the strain decreases in magnitude on almost the same path as the strain went up. However, when the pressure load is removed, the strains reverse direction while the mechanical load is held, indicating that the buckle in that bay has changed from outward (the exterior strain is in tension) to inward (the exterior strain is in compression). This change in deformation pattern is evident in the full-field measurements shown in Fig. 33, where the deformation at 110% DUL is shown with internal pressure and without internal pressure. All deformation half-waves are outward when internal pressure is present while, for the most part, the half-waves alternate in direction when pressure is not present.

Finally, the only other high strains are shown in Fig. 34 and 35, where strain in the crown is shown in the center frame web, and at the skin strain rosettes, respectively. The linear nature of the frame web behavior for strains on the front face and the back face indicates that the frame does not buckle. Strains on the webs of the center frame of the crown panel exhibit relatively high strains, as shown in Fig. 34. These strains remain linear throughout each phase of testing and do not indicate any buckling or rolling of the frames.

The mid-bay skin gauges whose results are shown for the up-bending load case are shown in Fig. 35 for the loading greater than DUL. Strains are greater than the design allowable, but no damage is evident. The maximum strain in the rosette is large, but does not show any indication of failures in this area. No visible damage growth was observed at any of the impact sites following the DUL or over-DUL tests. Additionally, ultrasonic scans performed in between loadings found no growth in damage compared to the damage found immediately following the impacts. A visual inspection of the entire box revealed no other damage.

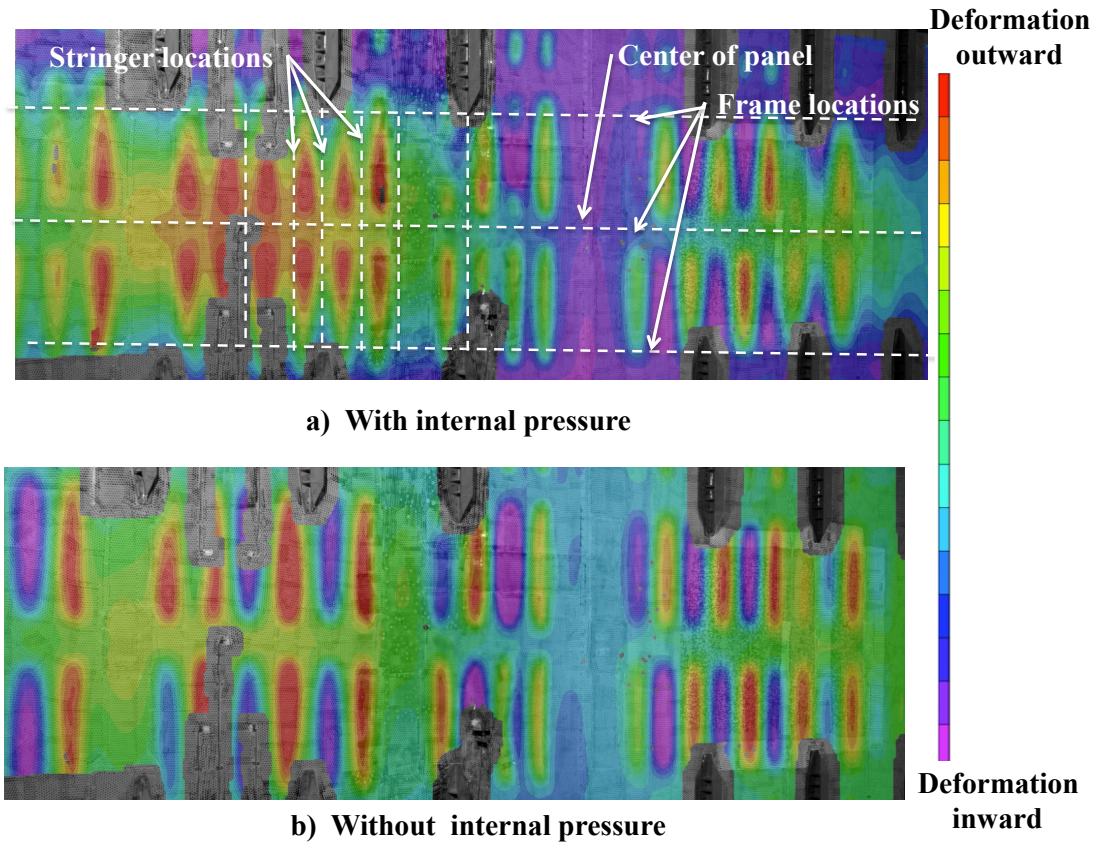

Figure 33. Crown out-of-plane deformation with a mechanical load of 110% DUL.

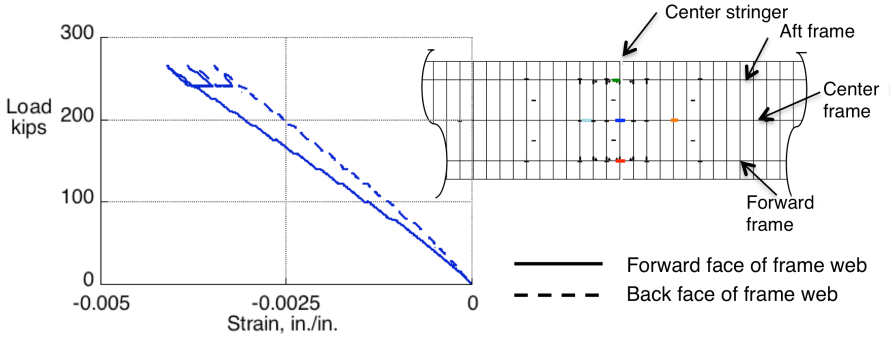

Figure 34. Strain in the crown frame web for the load case to a load greater than DUL.

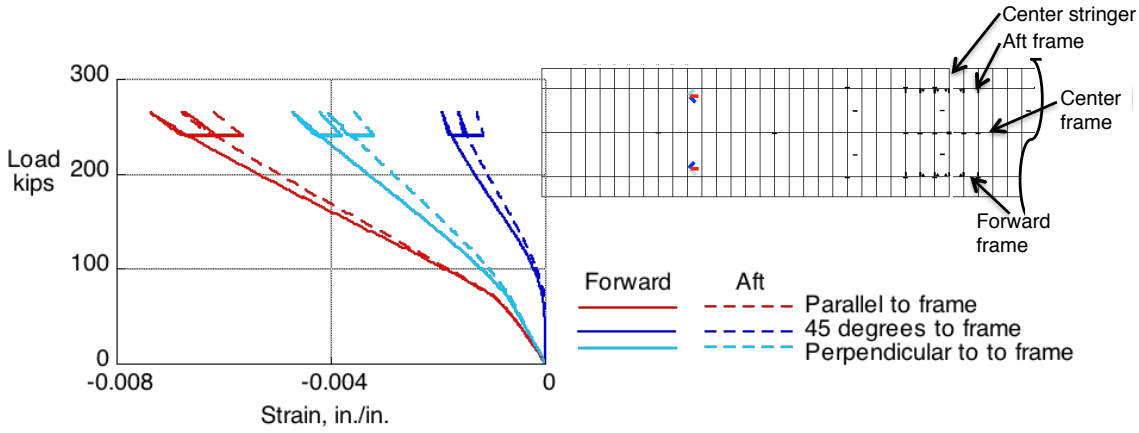

Figure 35. Strain in the crown skin strain rosettes load case to a load greater than DUL.

D. DSD

Since the test article displayed no damage growth from the impact sites and no damage elsewhere, an additional test was implemented. After the BVID tests were completed, the center frame in the crown panel was severed mid-bay to mid-bay, resulting in a 24-in. long cut. The entire depth of the web, the flanges and adjacent skin of the center frame were severed in a diamond shape, as shown in Fig. 36. A diamond shape, rather than a simple slot, was used because the edges would be pushed together during loading and contact between the cut edges was to be avoided. The ends of the cut were rounded and the cut through the frame height was tapered. Strain gauges were added to the interior skin and flanges in the vicinity of the DSD, the exterior was re-speckeled to accommodate a local VIC system, and then the structure was loaded in the up-bending load case to failure. With this level of damage, an aircraft structure would be required to support 70% of DLL, or approximately 47% DUL.

A detailed description of strain gauge results of the test article is presented in Ref. 29. Selected strain results are presented in Fig. 37-40. The locations of the gauges are shown in the figure using the colored boxes and the color of the curves in the plot correspond to the color of the boxes in the inset in a manner similar to that which was used in the previous sections. Some of the strain results show small abrupt changes in slopes in the strain-load plots due to the fact that the reacting platen did not rotate smoothly while load was applied. These discontinuities are not discussed herein.

The behavior of the test article was largely unaffected by the DSD away from the crown and upper bulkheads. The bulkhead and crown developed the same type of buckle patterns as discussed previously except in the region of the damage. Strain gauge results for gauges on the interior of the test article immediately adjacent to the DSD tips are shown in Fig 37. These results indicate that damage initiated at the tip at 130 kips and 132 kips, for the forward and aft tips, respectively. Then, damage grew to gauges immediately adjactent to these gauges at 154 kips and 173 kips, forward and aft, respectively. This behavior indicates that damage initiated on one side of the DSD, then initiated at the other side, then growth occurred at the first side, then at the second side. This damage growth did not immediately lead to damage to the stiffeners surrounding the damaged bay. This shifting of damage growth is consistent with the acoustic emission results.[29]

Strain gauge results in the damaged bay on the flanges of the surrounding frames and stringers are shown in Fig 38. The strains on the forward stringer flange are positive, indicating that the forward side of the bay deformed outward while strains on the aft stringer flange are negative indicating that the aft side of the bay deformed inward. A discontinuity is seen in the flange of the stringer toward the reacting platen on the forward side of the test article at a load of approximately 208 kips, indicating that a load redistribution took place at this load as damage progressed. Strains on the forward frame flange are more nonliner than the strains on the aft frame flange, however, both frame flanges are loaded in compression since the outer frames are the primary members supporting the compressive loads in the crown. The flange strain gauges did not fail until the final failure of the test article at approximately 242 kips, or 101% DUL.

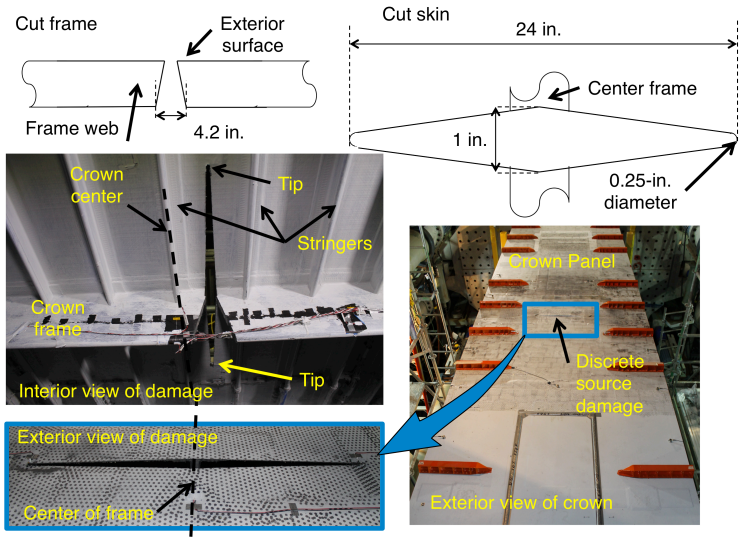

Figure 36. DSD geometry. Sketches not to scale.

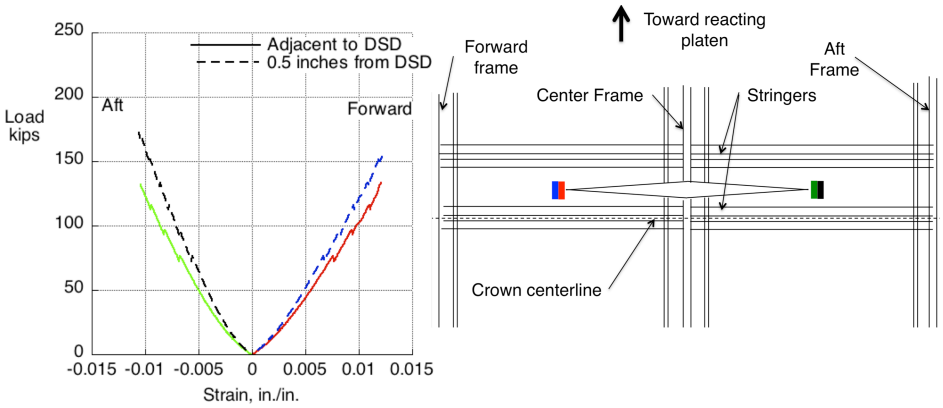

Figure 37. DSD tip strains. Sketch not to scale.

Strains further away from the damage on the forward and aft frames and at the T-caps are shown in Fig 39. The strains in the forward and aft T-caps were the same until a load of approx 150 kips, when one forward T-cap displayed an abrupt increase in strain. For load greater than 150 kips, all T-caps continued to support load with no addittional abrupt changes in strain behavior. This result indicates that a re-distribution of load occurred at this load level. Two strain gauges on each of the forward and aft frames show that the strain in the aft frame 21 inches from the centerline of the MBB in each direction agreed with each other. However, there is some difference due to the DSD between the forward frame 21 inches from the centerline of the MBB in each direction. However, the forward and aft frames behave in a similar manner.

Strains in the stringer webs near the DSD also show a behavior worth noting. Strain gauge rosettes were located on the stringer webs of the stringer adjacent to the DSD near the forward and aft frames. The rosette was oriented so that one leg was perpendicular to the skin and the other two were at $\pm 45^{o}$ to the skin. The strains measured by these rosettes are shown in Fig. 40 and indicate that the stringer near the forward flange recorded an abrupt change in strain at approximately 190 kips, but the results are mostly linear. The rosette at the aft frame, however, displays nonlinear behavior with a significant load redistribution at approximately 218 kips.

At approximately 242 kips, failure progressed through the forward and aft frames, through the forward and aft T-caps, and down into the forward and aft bulkheads. Additionally, when the center section of the crown panel could no longer support load, failures occurred in the crown and bulkheads near the inner ribs.

Therefore, it was determined that damage initiated at a load of approximately 130 kips and a series of damage progression steps occurred prior to the final failure at a load of 242 kips. It appears that damage arrested briefly at stitch lines, causing load redistribution during this process; however, this belief has not been proven conclusively at this time. Non-destructive inspection (NDI) results presented in Ref. 32 and 33 demonstrate that in the final failure sequence, damage stopped at the stitch lines in the bulkhead and crown panels. Photographs of the damage after failure of the test article are shown in Fig. 41 to Fig. 43.

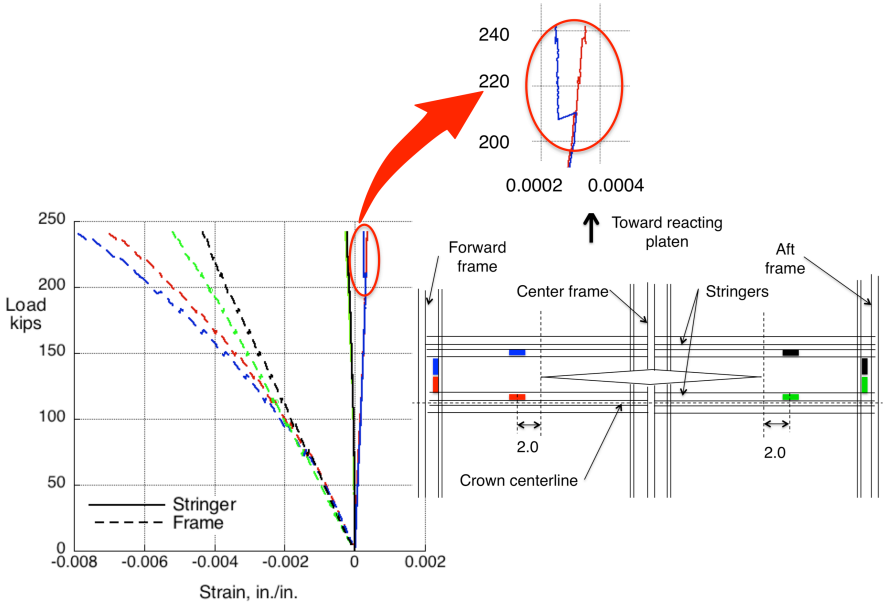

Figure 38. DSD bay flange strains. Sketch not to scale. Dimensions in inches.

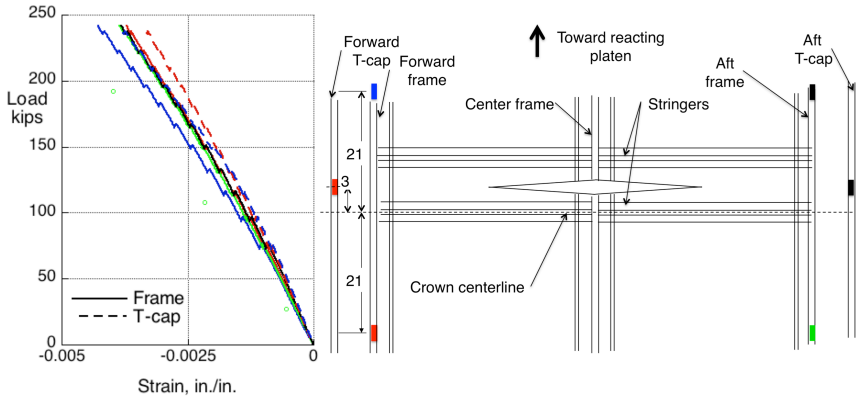

Figure 39. DSD region stiffener and T-cap strains. Sketch not to scale. Dimensions in inches.

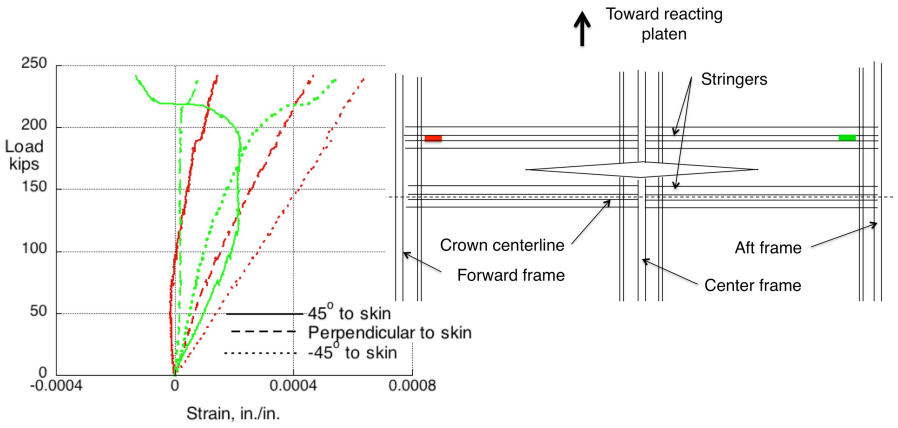

Figure 40. DSD region stringer web strains. Sketch not to scale.

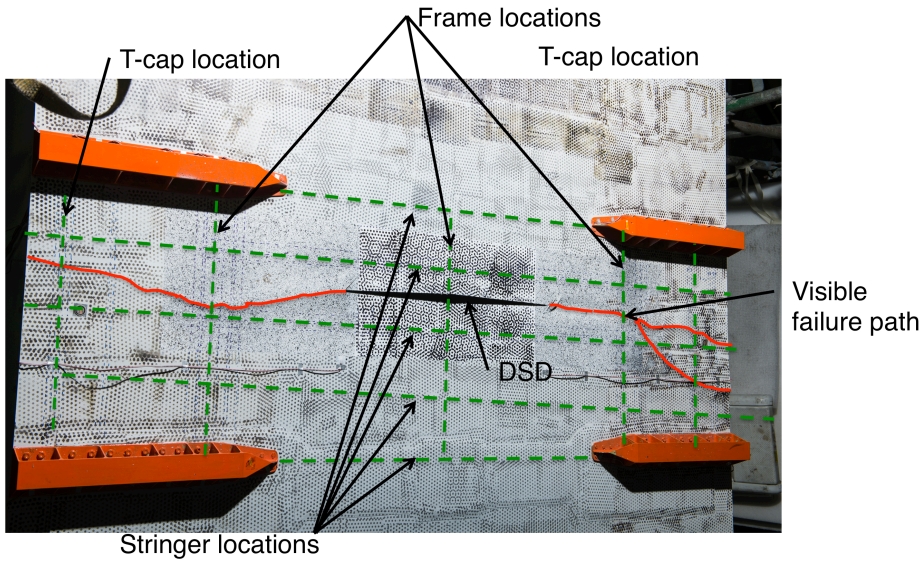

Figure 41. Exterior view of the DSD region.

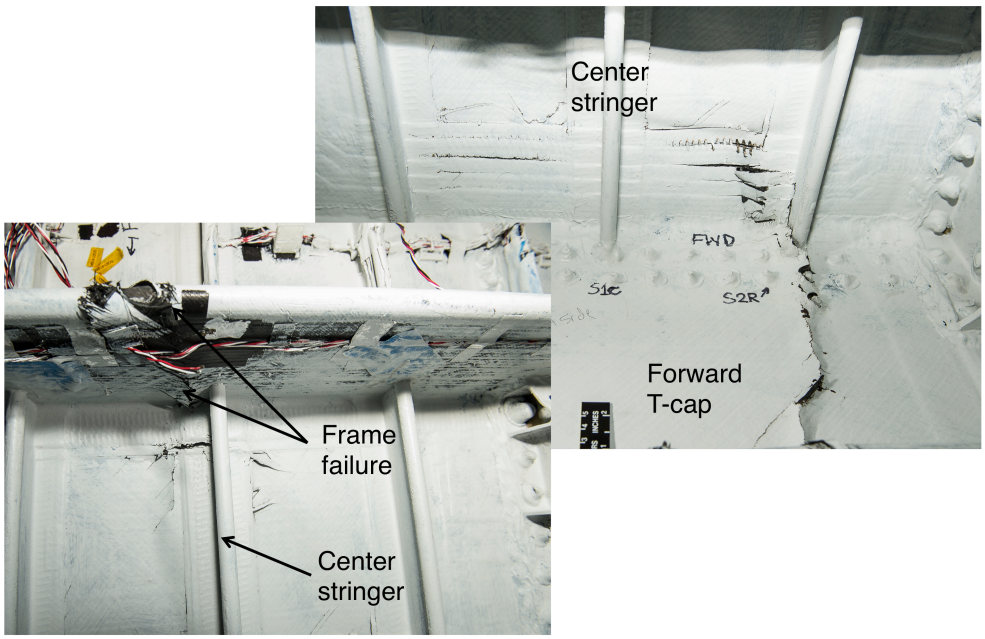

Figure 42. Interior view of failed frame in the DSD region.

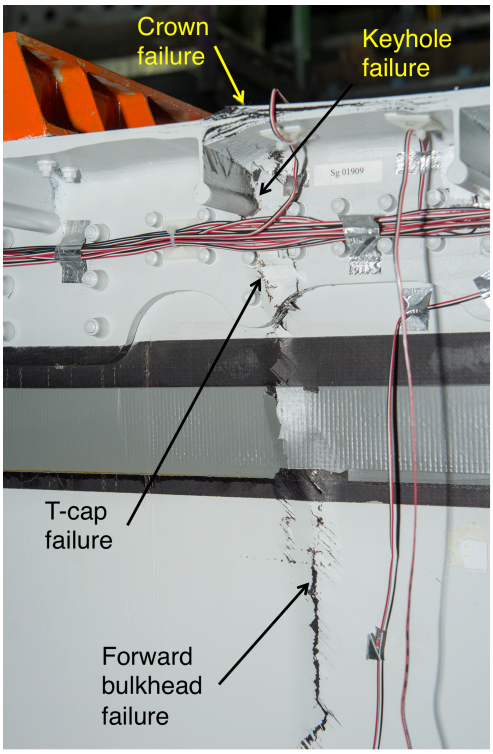

Figure 43. Failed bulkhead.

VIII. Concluding Remarks

For more than 20 years, NASA and The Boeing Company have been developing technology to improve damage tolerance and reduce the weight of composite structures for commercial transport aircraft applications through the use of through-the-thickness stitching. Most recently, under the NASA ERA Project, a partnership between NASA and Boeing has advanced this technology in an attempt to encourage and enable advanced aircraft configurations such as the HWB design.

Stitching through-the-thickness has been shown to suppress delaminations, arrest damage, and eliminate the need for fasteners in the acreage of composite panels. Removing the need for fasteners eliminates the need to drill holes, the need to add doublers to account for stress concentrations around holes, and the need to inspect fastener holes through the life of the aircraft.

In the current stitched structural concept, PRSEUS, the addition of a pultruded rod to the stringer in one direction and a tall foam-filled frame perpendicular to the stringer improves the bending stiffness in both directions compared to traditional construction, which is critical to the HWB configuration. PRSEUS also provides efficient load paths by integrating all panel elements into one unit prior to cure, which eliminates the need for shear clips and other added

elements that add weight to the structure. The PRSEUS panel architecture is a significant step beyond state-of-the-art conventional layered composite systems.

A building block test program starting with coupons and ending with a 30-foot-long large-scale pressure box test has been successfully executed to demonstrate the viability of a PRSEUS center body for the HWB transport aircraft. This final step in the building block process was the 80%-scale MBB tested in the COLTS Facility at NASA Langley Research Center. The MBB has been fabricated from PRSEUS panels and has undergone testing under combined load conditions representative of critical flight conditions. This test article has been subjected to up-bending and down-bending flight-maneuver load cases and internal pressurization in a ground-test program that demonstrates that the technology is capable of meeting the structural weight goals established for the HWB airframe. The test article was loaded to DUL in all critical conditions in the pristine conditions and then again after imparting BVID to the interior and exterior of the test article. The test article demonstrated post-buckling behavior as anticipated, and no damage growth from the impact sites was detected. All DUL testing has been completed and test results demonstrate the viability of the PRSEUS concept for HWB center section-type structure. The test article was loaded with DSD in the up-bending load case to demonstrate its ability to withstand large damage. With DSD in the form of a 24-inch-long notch, the test article supported DUL. The success of these tests indicates that there may be potential to modify the design since the test article supported loads greater than required. While this development program was aimed at demonstrating PRSEUS viability for the HWB center body, the benefits demonstrated could also be applied to traditional tube-and-wing aircraft configurations, other advanced configurations, spacecraft, and other structures where weight and through-the-thickness strength are design considerations.

Acknowledgments

The authors wish to acknowledge the team from Boeing who built the test article and worked with NASA supporting all the testing activities. We particularly want to acknowledge the work of Alex Velicki, Kim Linton, Tom Wu, Krishna Hoffman, Patrick Thrash, Jaime Baraja, Robert Pickell, and Andy Harbor. Their participation in the creation of the test article, planning, and implementation was critical to the success of the test program. The authors also wish to acknowledge Scott Simmons, Mike McNeil, Nate Gardner, Dave Dawicke, Scott Runnels, and the COLTS team for their support through the series of tests.

References

[1]Liebeck, R., "Design of Blended Wing Body Subsonic Transport," *Journal of Aircraft*, Vol. 41, No. 1, 2004, pp. 10-25.

[2]Velicki A., and Thrash P.J., "Advanced Structural Concept Development Using Stitched Composites," *Proceedings of the 49th AIAA/ASME/ASCE/AHS/ASC Structures, Structural Dynamics, and Materials Conference*, AIAA-2008-2329, Schaumburg, IL, April 2008.

[3]Jegley, D. C., Velicki, A., and Hansen, D. A., "Structural Efficiency of Stitched Rod-Stiffened Composite Panels with Stiffener Crippling," *Proceedings of the 49th AIAA/ASME/ASCE/AHS/ASC Structures, Structural Dynamics and Materials Conference*, AIAA-2008-2170, Schaumburg, IL, April 2008.

[4]Velicki, A., "Damage Arresting Composites for Shaped Vehicles, Phase I Final Report," NASA CR-2009-215932, 2009.

[5]Velicki, A., Yovanof, N. P., Baraja, J., Linton, K., Li, V., Hawley, A., Thrash, P., DeCoux, S., and Pickell, R., "Damage Arresting Composites for Shaped Vehicles – Phase II Final Report," NASA CR-2011-216880, 2011.

[6]Yovanof, N., and Jegley, D., "Compressive Behavior of Frame-Stiffened Composite Panels," *Proceedings of the 52nd AIAA Structures Dynamics and Materials Conference*, AIAA-2011-1913, Denver, CO, April 2011.

[7]Gould, K., Lovejoy, A., Jegley, D., Neal, A., Linton, K., Bergan, A., and Bakuckas Jr, J., "Nonlinear Analysis and Experimental Behavior of a Curved Unitized Stitched Panel," *Journal of Aircraft*, Vol. 52, No. 2, 2015, pp. 628-637.

[8]Jegley, D., "Structural Efficiency and Behavior of Pristine and Notched Stitched Structure," *presented at SAMPE Fall Technical Conference*, Fort Worth, TX, October 2011.

[9]Jegley, D., "Behavior of Frame-Stiffened Composite Panels with Damage," *Proceedings of the* 54th *AIAA/ASME/ASCE/AHS/ASC Structures, Structural Dynamics and Materials Conference*, AIAA-2013-1738, Boston, MA, April 2013.

[10]Lovejoy, A., Rouse, M., Linton, K., and Li, V., "Pressure Testing of a Minimum Gauge PRSEUS Panel," *Proceedings of the 52nd AIAA Structures Dynamics and Materials Conference*, AIAA-2011-1813, Denver, CO, April 2011.

[11]Yovanof, N., Baraja, J, Lovejoy, A., and Gould, K., "Design, Analysis, and Testing of a PRSEUS Pressure Cube to Investigate Assembly Joints," *Proceedings of the 2012 Aircraft Airworthiness and Sustainment Conference*, TP5431, Baltimore, MD, April 2012.

[12]Przekop, A. and Jegley, D. C., "Evaluation of a Metallic Repair on a Rod-Stiffened Compsite Panel," *Journal of Aircraft*, Vol. 51, No. 3, 2014, pp. 792-804.

[13]Jegley, D. C., Rouse, M., Przekop, A., and Lovejoy, A. E., "The Behavior of a Stitched Composite Large-Scale Multi-Bay Pressure Box," NASA TM-2015-218972, 2015.

[14]Przekop, A., Jegley, D.C., Rouse, M., and Lovejoy, A.E., "Finite Element Analysis and Test Results Comparison for the Hybrid Wing Body Center Section test Article," NASA TM-2015-218973, 2015.
[15]Velicki, A., "Damage Arrest Design Approach with Composite Materials," *presented at the Aging Aircraft Conference*, Kansas City, KA, May, 2009.
[16]Velicki, A. and Thrash, P., "Damage Arrest Design Approach Using Stitched Composites," *presented at the 2nd Aircraft Structural Design Conference*, London, England, October, 2010,
[17]Linton, K., Velicki, A., Hoffman, K., Thrash, P., Pickell, R., and Turley, R., "PRSEUS Panel Fabrication Final Report," NASA-CR-2014-218149, January 2014.
[18]Thrash, P., "Manufacturing of a Stitched Resin Infused Fuselage Test Article," *presented at SAMPE Fall Technical Conference*, Dallas, TX, October 2014
[19]Velicki, A., Linton, K., and Hoffman, K., Final Report for "Fabrication of Lower Section and Upper Forward Bulkhead Panels of the Multi-bay Box and Panel Preparation," NASA-CR-2015-21981, November 2015.
[20]Velicki, A., Hoffman, K., Linton, K., Baraja, J., Wu, H., Thrash, P., "Hybrid Wing Body Multi-Bay Test Article Analysis and Assembly," Final Report, Contract NNL10AA05B, Task Order NNL11AA68T, July 2015.
[21]Wu, H.T., Shaw, P., and Przekop, A., "Analysis of a Hybrid Wing Body Center Section Test Article," *Proceedings of the 54th AIAA/ASME/ASCE/AHS/ASC Structures, Structural Dynamics and Materials Conference*, AIAA-2013-1734, Boston, MA, April 2013.
[22]Przekop, A., Wu, H. T., and Shaw, P., "Nonlinear Finite Element Analysis of a Composite Non-Cylindrical Pressurized Aircraft Fuselage Structure," *Proceedings of the 55th AIAA/ASME/ASCE/AHS/ASC Structures, Structural Dynamics and Materials Conference*, AIAA-2014-1064, National Harbor, MD, January, 2014.
[23]Ambur, D. R., Rouse, M., Starnes, J. H., and Shuart, M. J., "Facilities for Combined Loads Testing of Aircraft Structures to Satisfy Structural Technology Development Requirements," *presented at the 5th Annual Advanced Composites Technology Conference*, Seattle, WA, August, 1994.
[24]Rouse, M., "Methodologies for Combined Loads Tests Using a Multi-Actuator Test Machine," *presented at the Society for Experimental Mechanics meeting*, Chicago, IL, June 2013.
[25]Rouse, M. and Jegley, D., "Preparation for Testing a Multi-Bay Box Subjected to Combined Loads," *presented at the Society for Experimental Mechanics meeting*, Costa Mesa CA, June 2015.
[26]Moore, J. P., Przekop, A., Juarez, P. D., and Roth, M. C., "Fiber Optic Rosette Strain Gauge Development and Application on a Large-Scale Composite Structure," NASA TM-2015-218970, 2015.
[27]Horne, M.R., "Acoustic Emission Results for the PRSEUS Multi-Bay Box Testing," NASA TM-2015-21876, 2015.
[28]Przekop, A., Jegley, D., Rouse, and Lovejoy, A. "Testing and Analysis of a Composite Non-Cylindrical Aircraft Fuselage Structure, Part I: Ultimate Design Loads," *Proceedings of the 57th AIAA/ASME/ASCE/AHS/ASC Structures, Structural Dynamics and Materials Conference*, San Diego, CA, January 2016.
[29]Przekop, A., Jegley, D., Rouse, and Lovejoy, A. "Testing and Analysis of a Composite Non-Cylindrical Aircraft Fuselage Structure, Part II: Severe Damage," *Proceedings of the 57th AIAA/ASME/ASCE/AHS/ASC Structures, Structural Dynamics and Materials Conference*, San Diego, CA, January 2016.
[30]McGowan, D. M., Ambur, D. R., and McNeil, S. R., "Full-field Structural Response of Composite Structures: Analysis and Experiment," *Proceedings of the 44th AIAA/ASME/ASCE/AHS/ASC Structures, Structural Dynamics and Materials Conference*, AIAA 2003-1623, Norfolk, VA, April 2003.
[31]Lovejoy, A., and Przekop, A., "Imparting Barely Visible Impact Damage to a Stitched Composite Large-Scale Pressure Box," *Proceedings of the 57th AIAA/ASME/ASCE/AHS/ASC Structures, Structural Dynamics and Materials Conference*, San Diego, CA, January 2016.
[32]Johnston, P. H. and Juarez, P. D., "Nondestructive Evaluation of PRSEUS During Large-Scale Load Testing and Rod Push-Out Testing," NASA TM-2015-218978, 2015.
[33]Johnston, P. H. and Juarez, P. D., "Nondestructive Evaluation of PRSEUS During Large-Scale Load Testing and Rod Push-Out Testing," *Proceedings of the 57th AIAA/ASME/ASCE/AHS/ASC Structures, Structural Dynamics and Materials Conference*, San Diego, CA, January 2016.